From deep to shallow fluid reservoirs: evolution of fluid sources during exhumation of the Sierra Almagrera, Betic Cordillera, Spain

Vanessa Dyja, Christian Hibsch, Alexandre Tarantola, Michel Cathelineau, Marie-Christine Boiron, Christian Marignac, Daniele Bartier, Javier Carrillo-Rosúa, Salvador Morales Ruano, Philippe Boulvais

GEOFLUIDS

From deep to shallow fluid reservoirs: evolution of fluid sources during exhumation of the Sierra Almagrera (Betics, Spain)

Journal:	*Geofluids*
Manuscript ID:	Draft
Manuscript Type:	Original Manuscript
Date Submitted by the Author:	n/a
Complete List of Authors:	Dyja, Vanessa; GeoRessources, Université de Lorraine, CNRS, CREGU, UMR 7359 Hibsch, Christian; GeoRessources, Université de Lorraine, CNRS, CREGU, UMR 7359 Tarantola, Alexandre; GeoRessources, Université de Lorraine, CNRS, CREGU, UMR 7359 Cathelineau, Michel; GeoRessources, Université de Lorraine, CNRS, CREGU, UMR 7359 Boiron, Marie-Christine; GeoRessources, Université de Lorraine, CNRS, CREGU, UMR 7359 Marignac, Christian; GeoRessources, Université de Lorraine, CNRS, CREGU, UMR 7359 Bartier, Danièle; GeoRessources, Université de Lorraine, CNRS, CREGU, UMR 7359 Carrillo-Rosúa, Javier; Universidad de Granada, Facultad de Ciencias, Mineralogia y Petrologia Morales, Salvador; Universidad de Granada, Facultad de Ciencias, Mineralogia y Petrologia Boulvais, Philippe; Géosciences Rennes, Université de Rennes, UMR CNRS 6118, OSUR,
Key words:	Metamorphic Core Complex, Metamorphic brines, Fluid inclusions, Stable isotopes, Betic Cordillera, Trans-alboran fault

From deep to shallow fluid reservoirs: evolution of fluid sources during exhumation of the Sierra Almagrera (Betics, Spain)

Vanessa Dyja [a], Christian Hibsch [a], Alexandre Tarantola [a], Michel Cathelineau [a], Marie-Christine Boiron [a], Christian Marignac [a], Danièle Bartier [a], Javier Carrillo-Rosúa [b], Salvador Morales Ruano [b] and Philippe Boulvais [c]

[a] GeoRessources, Université de Lorraine, CNRS, CREGU, UMR 7359, Vandœuvre-lès-Nancy, F-54506, France

[b] Facultad de Ciencias de la Educación, Campus de Cartuja, 18071, Granada, Spain

[c] Université de Rennes 1, Géosciences Rennes - UMR CNRS 6118, OSUR, 35042 Rennes Cedex, France

Corresponding Author:

E-mail address: vanessa.dyja@univ-lorraine.fr
Postal address: GeoRessources, UMR 7359, Université de Lorraine, boulevard des Aiguillettes, 54506 Vandœuvre-lès-Nancy, France
Tel: +33 3 83 68 47 46
Fax: +33 3 83 68 47 01

Keywords

Metamorphic Core Complex / Metamorphic brines / Fluid inclusions / Stable isotopes / Betic Cordillera / Trans-alboran fault

Abstract

The combination of structural, geochemical and paleotopographic data proves to be an efficient tool to understand fluid transfers in the crust. This study discriminates shallow and deep fluid reservoirs on both sides of the brittle-ductile transition under an extensional regime, and points out the role of major transcurrent fault activity in this paleo-hydrogeological setting.

Paleo-fluids trapped in quartz and siderite-barite veins record the transfer of fluids and metal solute species during the Neogene exhumation of the Sierra Almagrera metamorphic belt. Ductile then brittle-ductile extensional quartz veins formed from a deep fluid reservoir, trapping metamorphic secondary brines containing low-density volatile phases derived from the dissolution of Triassic evaporites. During exhumation, low-salinity fluids percolated within the brittle domain, as shown by transgranular fluid inclusion planes affecting previous veins. These observations indicate the opening of the system during Serravalian to early Tortonian times, and provide evidence for the penetration of surficial fluids of meteoric or basinal origin into the upper part of the brittle-ductile transition.

During exhumation, synsedimentary transcurrent tectonic processes occurred from Late Tortonian times onwards, while marine conditions prevailed at the Earth's surface. At depth in the brittle domain, quartz veins associated with hematite record a return to high-salinity fluid circulation suggesting an upward transfer fed from the lower reservoir. During the Messinian, ongoing activity of the Trans-Alboran tectono-volcanic trend led to the formation of ore deposits.

Reducing fluids led to the formation of siderite and pyrite ores. The subsequent formation of galena and barite may be related to an increase of temperature. The high salinity and Cl/Br ratio of the fluids suggest another source of secondary brine derived from dissolved Messinian evaporites, as corroborated by the $\delta^{34}S$ signature of barite. This constrains the age of the mineralizing event at around 5.65 Ma, prior to the main Messinian salinity crisis.

1. Introduction

Fluids are vectors of heat and solute species. Migration of fluids is linked to local and regional geology, and permeability is a key factor in controlling fluid flow (Manning & Ingebritsen, 1999, Ingebritsen & Manning, 2002). Permeability is a function of time, heterogeneity-anisotropy and scale (Manning & Ingebritsen, 1999). The Sierra Almagrera (southern Spain) is a favourable terrain to evaluate the conditions of fluids migration within the Earth's lithosphere. Because this

area is located in a context of exhumation disturbed by the trans-Alboran transcurrent fault system, fluid flows can be studied through time across the brittle-ductile transition.

Fluid analysis can focus on the exhumation of metamorphic rocks occurring in wedges undergoing active thickening, owing to the intense erosion of the hanging-wall overlying thrust systems (Menzies *et al.*, 2014). Within Basin and Range type provinces, studies of fluids can also elucidate the exhumation of rocks from the footwall during thinning processes as revealed by the presence of crustal detachments associated with low-angle and high-angle normal faults (Wernicke & Burchfiel, 1982, Lister & Davis, 1989, Vanderhaeghe & Teyssier, 2001). In both geological settings, the location of the brittle-ductile transition plays a major role. In extensional settings, this rheological transition may localize detachment and decollement layers where normal faults are generally rooted. There is currently much debate about the hydrogeological role of the brittle-ductile transition. The rheological change occurring at this transition may separate a deep reservoir, which is accessible to metamorphic and/or magmatic and mantle fluids confined under lithostatic conditions, from a shallower reservoir accessible to surficial fluids (meteoric, marine or basinal) circulating under lithostatic to hydrostatic conditions (Morrison & Anderson, 1998, Famin & Nakashima, 2004). These two reservoirs may interact through tectonic and magmatic processes. Surficial fluids may reach the upper part of the deeper reservoir under contractional regimes (Menzies *et al.*, 2014) as well as under extensional regimes (Mulch *et al.*, 2004, Famin *et al.*, 2005, Siebenaller *et al.*, 2013). Alternatively, deeper fluids may access the upper brittle crust and mix with fluids closer to the Earth's surface (Boiron *et al.*, 2003), a process which may also be triggered by magma ascent. Such fluid circulation events are commonly associated with hydrothermal processes (metasomatism and mineralization) (Beaudoin, 1994), and it is then necessary to decipher the role played by the different reservoirs and fluids during the tectonic and magmatic events.

The convergence between Africa and Europe resulted in a complex geotectonic history with subduction of upper continental crust (Eocene to Middle Miocene), followed by extensional tectonics. This early extension triggered the exhumation of metamorphic cores in the internal zones

of the Betic cordillera during the Miocene (between 18 to 14 Ma: Gomez-Pugnaire *et al.* (2004), Platt *et al*. (2006) and Gomez-Pugnaire (2012), and possibly even earlier (Augier *et al.*, 2005b). Further exhumation has occurred under compressional regimes since the late Miocene due to erosional processes affecting the uplifting metamorphic cores. The different mountain ranges have been also partly dissected by a major transcurrent fault system, which has led to the formation of synsedimentary continental to marine basins (Weijermars, 1985, Booth-Rea *et al.*, 2003). Volcanism occurred later in the evolution of the Betics, reflecting mantle and crust processes as well as mantle-crust interactions at depth (e.g. Benito *et al.* (1999); Turner *et al.* (1999); Duggen *et al.* (2004)). A major erosional event allowed the uplift of ranges during the Messinian salinity crisis. Deposition of evaporites in the central Mediterranean Sea and incision features affected the bordering slopes. Prior to the main sea-level drop (5.60-5.46 Ma), a first stage of deposition of evaporites with controversial ages (7.20 Ma / 5.96-5.67 Ma) has been recorded in some basins of the Betics (Fortuna, Lorca, Guadix-Baza, Granada and Sorbas) (Clauzon, 1980, Gautier *et al.*, 1994, Garcés *et al.*, 1998, Rouchy *et al.*, 1998, Krijgsman *et al.*, 1999, Seidenkrantz *et al.*, 2000, Krijgsman *et al.*, 2000, Gargani *et al.*, 2008, Bourillot *et al.*, 2009, Omodeo Salé *et al.*, 2012).

The Sierra Almagrera metamorphic core exhibits a sequence of quartz vein formation. A series of siderite and barite base metal-bearing ore veins, as well as quartz and carbonate barren veins in the brittle domain, are associated with the transcurrent tectonics. Study of the different fluids trapped as inclusions in this vein sequence allows the characterization of the deep reservoir fluids in equilibrium with the rocks during the ductile stage and the evolution of the fluids within the same reservoir during its exhumation towards exposure at the present day. This reservoir was subject to different deformation styles, from ductile to brittle, and records the Neogene evolution of this part of the Betic orogenic wedge.

In this study, we combine structural, paleogeographical and geochemical data to propose a scenario of hydrogeological evolution during exhumation across the brittle-ductile transition in the Sierra Almagrera. In addition, we discuss the hydrogeological influence of the brittle ductile

transition on the lower and upper crustal reservoirs during the Miocene extensional tectonics, the effect of transcurrent deformation on the hydrogeological configuration, the possible fluid sources at the various stages of this evolution and the timing of mineralizations in the region.

2. Geological context

2.1. The Betic Cordillera (SE Spain)

The Betic Cordillera results from the convergence between the Africa and Eurasia plates since the Eocene, and forms an alpine tectonic wedge reaching a thickness of about 60 km (Platt & Vissers, 1989, Lonergan & White, 1997, Platt, 2007, Jolivet et al., 2008). The internal Alboran domain can be divided into three main tectono-metamorphic nappes, from bottom to top (Figure 1): (i) the Nevado-Filábride nappe, itself divided into three sub-units from bottom to top: Ragua (not represented on Figure 1, to the W), Calar-Alto and Bedar-Macael (De Jong, 1991, Martínez-Martínez et al., 2002), (ii) the Alpujarride nappe, and (iii) the Malaguide nappes (Egeler & Simon, 1969). In addition to isostatic uplift, these units were also exhumed due to tectonic unroofing (Lonergan & Mange-Rajetzky, 1994). The associated WSW-ENE-striking tectonic extension related to exhumation of the metamorphic continental crust is supposed to have resulted from partial or complete removal of the lithospheric mantle (Platt & Vissers, 1989). Arguments have also been put forward for other mechanisms, such as subduction zone rollback (Lonergan & White, 1997, Bezada et al., 2013). The contacts observed between structural units exhibiting different degrees of metamorphism are attributed to major detachment faults (Figure 1-a): (1) The Malaguide-Alpujarride contact: unmetamorphosed Malaguide lithologies overlie the medium-pressure medium-temperature metamorphic rocks of the Alpujarride nappe (Sierra Estancias, Figure 1-a), (2) The Filabres major detachment: higher grade Nevado-Filábride metamorphic rocks, which were exhumed during the Miocene, lie beneath the Alpujarride nappes. Ductile shearing related to this exhumation affected the footwall and currently shows a transport direction top towards WSW to SW (Crespo-Blanc et al., 1994, Martínez-Martínez & Azañón, 2002, Platt, 2007). According to the extensional tectonics expressed in the ductile fabrics, the metamorphic nappes reached the brittle

domain during the ongoing exhumation. From the late Miocene, exhumation was mainly the result of erosion since both the metamorphic cores and the sedimentary cover were affected by regional compressional and local transcurrent tectonics. The Trans-Alboran transcurrent fault system generated domains with both releasing and restraining deformation, which created juxtaposed zones with opposite vertical motions (subsidence and uplift). The ranges (sierras) were separated by basins either filled by continental or marine sediments according to time and location. This major tectono-volcanic trend can be followed off-shore to the other side of the Mediterranean in Morocco (Hernandez et al., 1987).

The volcanism linked to lithospheric thinning shows a gradual transition and great geochemical diversity. The age of this volcanism varies from 34 Ma (tholeiitic dykes in Malaga province) to 2 Ma (alkali basalts in Murcia province). There is a gap between the oldest volcanic events in Malaga and the main magmatic activity in SE Spain and the Alboran Basin, which took place between 12.6 and 7.5 Ma with tholeiitic and calc-alkaline affinities (Bellon *et al.*, 1983). Very locally in the Sierra Cabrera, Miocene plutonism is recorded related to the retrograde metamorphism and associated ductile deformation (Westra, 1969, Bolze *et al.*, 1986). Since the reappearance of volcanism during the Serravalian, other episodes of magmatic activity occurred inland in SE Spain mainly between 10 and 6.2 Ma, showing high-K calc-alkaline, shoshonitic and ultrapotassic affinities (Bellon *et al.*, 1983, Turner *et al.*, 1999, Zeck *et al.*, 2000, Duggen *et al.*, 2004, Duggen *et al.*, 2005, Cesare *et al.*, 2009). Heterogeneous sources and various processes are implied in the magma genesis, including: (i) various degrees of partial melting, (ii) metasomatism (i.e. oceanic and continental crust, sediments), (iii) anatexis of crustal metasedimentary basement (Benito *et al.*, 1999, Duggen *et al.*, 2004, Duggen *et al.*, 2005, Prelevic *et al.*, 2008, Álvarez-Valero & Kriegsman, 2008, Conticelli *et al.*, 2009).

The Neogene evolution of the Betics is associated with a series of base and precious metal-bearing hydrothermal ore systems developed mainly in the calc-alkaline volcanic rocks of the Cabo de Gata range, but also in sedimentary and metamorphic basement lithologies (Figure 1).

Epithermal ore deposits are hosted by intermediate to acid volcanics ranging in age from 12 to 10 Ma; these deposits are found in a number of different mining districts, for example, Zn-Pb-Cu(-Ag-Au) at San José (Demoustier *et al.*, 1998, Esteban-Arispe *et al.*, 2009), Au(-Cu-Te-Sn) at Rodalquilar (Arribas *et al.*, 1995) and Cu-Au-Ag at Carboneras (Morales Ruano *et al.*, 2000, Carrillo-Rosúa *et al.*, 2009). Ba-Ag mineralizations are found in sedimentary rocks, close to high-K calc-alkaline and shoshonitic volcanics within the Vera Basin (Alvado, 1986, Martínez-Frías, 1998). Certain ore deposits are hosted by metamorphic rocks, including the occurences of Pb-Zn-Fe-Cu (Al) at Cartagena (Graeser & Friedrich, 1970, Oen *et al.*, 1975, Arribas *et al.*, 1983) and Pb-Zn-Ag-Fe at Sierra Almagrera and Sierra Aguilon (Martinez Frias *et al.*, 1989, Morales Ruano *et al.*, 1993). Samples from the Sierra Almagrera mining distict allow us to reconstruct the fluid history described below.

2.2. Geology of the Sierra Almagrera (Figure 1-b)

The metamorphic range of the Sierra Almagrera exposes a Nevado Filabres unit largely composed of graphitic quartz-rich chloritoid-schists (Booth-Rea *et al.*, 2004) and quartzites. Locally, carbonates and gypsum are found north of the Sierra Almagrera within an Alpujarride unit (Álvarez & Aldaya, 1985). The present-day geomorphology of the Sierra Almagrera mainly results from sinistral strike-slip faulting in the area that generated several fault segments at various scales. The Palomares Fault Zone results in an approximately 16 km North-South trending left-lateral relative displacement (Booth-Rea *et al.*, 2004). This transcurrent faulting may have started during the late Tortonian (around 7.2 Ma), but was mainly active during the Messinian. The evolution of this faulting associated with a vertical component (oblique faulting) caused the recent uplift, thus leading to erosion and exhumation of the Sierra Almagrera during the Plio-Quaternary. The southern segments of the Palomares Fault Zone dip towards the West. Their transtensional activity favoured the subsidence of the western block. By contrast, the northern segments, which are dipping towards the ESE, are related to a sinistral restraining bend that favoured the uplift of the Sierra Almagrera mountain ranges located to the East of the zone (Booth-Rea *et al.*, 2004). In the

studied area, small bodies of high-K calc-alkaline to shoshonitic rhyodacites (Lopez Ruiz & Rodriguez Badiola, 1980, Benito *et al.*, 1999) are encountered along the transcurrent fault system. Regional ages determined on this volcanic suite are between 11.9 and 6.2 Ma (Duggen *et al.*, 2004). Less abundant lamproites from the ultrapotassic series (Lopez Ruiz & Rodriguez Badiola, 1980), dated at between 8.4 and 6.4 Ma (Prelevic *et al.*, 2008), crop out within the Vera basin to the south of Sierra Almagrera (Figure 1-b).

Mineralizations in the Sierra Almagrera are found in veins within the metamorphic rocks of the currently uplifted metamorphic range (Figure 1-b). In the present study, this formerly exploited area is referred to as the Sierra Almagrera mining district. While some mineralised veins are exposed at outcrop in the Sierra, the sulphides are frequently oxidized. Non-altered veins can still be sampled along the E-W striking horizontal gallery at El Arteal. Subvertical fractures filled by siderite, barite, hematite and ore minerals crosscut the metamorphic fabric of graphitic schists and quartz veins transposed or partly transposed within the main rock foliation. Our study shows that the mineralised fractures are arranged in two main clusters striking N160°-N180° and N120°-N130° (Figure 1-c).

The area located within the Palomares Fault Zone (hanging-wall) is referred to here as "the subsident area". Locally, mineralizations can be found within the Messinian sediments (Las Herrerias). The ore consists of barite veins, with native Ag and base-metal sulphides in very small amounts (Alvado, 1986, Martínez-Frías, 1998, Carrillo-Rosúa *et al.*, 2002, 2003).

3. Methods

3.1. Fluid inclusion investigations

3.1.1 Fluid inclusion petrography

Double-polished 150-200-µm-thick sections were prepared for microscopic and microthermometric observations of mineralized veins of quartz, siderite, barite and calcite. The sections were oriented (using azimuth convention) to determine present-day strike and dip of fluid

inclusion planes. Isolated fluid inclusions or clusters are interpreted as primary. Intragranular fluid inclusion planes are found within single grains in microcracks that do not cross-cut grain boundaries (Van Den Kerkhof & Hein, 2001). Transgranular fluid inclusion planes result from healing of former open cracks (Krantz, 1983, Boullier, 1999, Lespinasse, 1999, Lespinasse *et al.*, 2005) as rocks undergo brittle deformation. Systematic measurements of the fluid inclusion planes were carried out on each section using an ANIMA interactive videographic image analyzer (Lespinasse *et al.*, 2005). The plunge and dip directions of the fluid inclusion planes are represented on equal-area lower-hemisphere stereograms using Stereonet® software.

3.1.2 Microthermometry

The phase transitions of the fluid inclusions were characterised between –170 °C and +600 °C using a LINKAM MDS 600 heating-freezing stage mounted on an Olympus microscope, calibrated using CO_2 and H_2O synthetic and natural alpine fluid inclusions. The accuracy of measurements varies from ±0.2 °C at low temperature (experiments at 0.5-1 °C/min) to ±2 °C at high temperature (experiments at 1-5 °C/min). Table 1 reports the abbreviations of terms and the phase transition temperatures observed during microthermometric experiments. For barite and calcite, the high-temperature transitions were studied first to prevent leakage of fluid inclusions during ice formation on cooling. Photographs of fluid inclusions after each measurement were compared with the original picture to evaluate any leakage.

3.1.3 Raman microspectroscopy

Raman analysis of fluid inclusions was performed with a LabRAM microspectrometer (Horiba Jobin Yvon, at GeoRessources, Vandœuvre-lès-Nancy, France) equipped with a 1800 $gr.mm^{-1}$ grating and a ×80 Olympus objective. The exciting radiation was provided by the 514.5 nm line of an Ar^+ laser (Stabilite 2017, Newport Corp., Spectra Physics) at a power of 400 mW. The signal-to-noise ratio was optimized by adjusting acquisition time and accumulation number. The quantitative analysis of the gas phase was performed using a specific calibration of the laboratory. Results are given as mol% relative to the volatile phase.

3.1.4 P-V-T-X calculation of fluid inclusions

In this study, we use microthermometric data associated with mole fractions of the different gas species obtained by Raman spectroscopy to reconstruct the *P-V-T-X* evolution of fluid inclusions. The salinities of aqueous fluid are calculated using the final melting temperature of ice when gases are not present in sufficient amounts to form gas hydrates (Bodnar, 2003). In this case, the isochore is a function of the homogenization temperature at a given salinity, and the empirical equation of state of Zhang and Frantz (1987) is used within a *P-T* domain of validity of *T*: 180-700 °C and *P*: 0.1-300 MPa.

The salinities of aqueous carbonic fluids and molar volumes (V_m) of the volatile phase are calculated using the program ICE and the dissociation temperature of clathrate (Bakker, 1997, 2003) when gases are present in significant amounts to allow the formation of gas hydrates. The isochores are calculated using the program ISOC (Bakker, 1997, 2003) and the equation of state (Bowers & Helgeson, 1983) revised by Bakker (1999) for the system H_2O-CO_2-CH_4-N_2-NaCl, with a *P-T* domain of validity of *T*: 350-600 °C and *P*: 50-200 MPa.

3.1.5 Crush-leach analysis for halogen chemistry

Because the halogens display a conservative behaviour in solution, and remain relatively unaffected by fluid-rock interactions (Banks *et al.*, 1991), the signature of the elements Cl and Br in a fluid can be used to characterize its source (Böhlke & Irwin, 1992).

Bulk crush-leach analyses were performed to extract and analyse fluids hosted in quartz, barite and siderite. Samples were prepared according to the methodology of Bottrell et al. (1988). The amount of sample crushed was between 0.5 and 1.0 g. Analysis of the anions F, Cl, Br, I and SO_4 was performed by ion chromatography using a ICS 3000 Dionex system with a AS20 column at the LIEC laboratory (Nancy, France). Br was also analysed by LA-ICPMS in a series of representative fluid inclusions using the procedure described by Leisen et al. (2012a).

3.1.6 Laser Ablation ICP-MS

This technique allows direct ablation of individual fluid inclusions within the host mineral, represented in the present study by quartz, siderite and barite. The LA-ICP-MS instrument (GeoRessources laboratory, Vandœuvre-lès-Nancy, France) comprises a GeoLas excimer laser (ArF, 193 nm, Microlas, Göttingen Germany) and an Agilent 7500c quadrupole ICP-MS equipped with an octopole reaction-cell using H_2 gas, and a collision-cell using He gas. The laser beam is focused onto the sample within an ablation cell with a Schwarzschild objective (magnification x25) linked with a CCD camera. Synthetic glass provided by the National Institute of Standards and Technology (NIST) is used for calibration of the different analysed elements and respective masses (200 pulses at 5 Hz). The design as an optical imaging system allows the use of different crater diameters (24, 32 or 60 µm) at constant energy density on the sample, by adjusting an aperture in the laser beam path. Na, K, Mg, Ba, Sr, Mn, Li, Fe, Cu and Zn are analysed here. Concentrations are calculated according to Leisen *et al.* (2012b).

3.2. Raman spectroscopy of carbonaceous materials

The Raman Spectrum of Carbonaceous Material (RSCM) has been calibrated as a geothermometer in the range 330-640 °C (Beyssac *et al.,* (2002, 2004)). The RSCM displays one graphite band (G band) and several defect-activated bands (D1 and D2 bands) between 1100 and 1800 cm^{-1} (Beyssac & Lazzeri, 2012), whose intensities decrease with increasing metamorphic grade. Raman analysis of graphite-bearing schists was performed on thin sections oriented perpendicular to the foliation and parallel to the lineation by focusing the laser beam beneath a transparent crystal to avoid the effect of amorphization due to polishing. The Raman spectrometer used in this study is a LabRAM HR instrument (Horiba Jobin Yvon) (GeoRessources, Vandœuvre-lès-Nancy, France) equipped with a 600 $gr.mm^{-1}$ grating and a ×100 objective (Olympus). The excitation beam is provided by an Ar^{+} laser (Stabilite 2017, Newport Corp., Spectra Physics) at 457.9 nm. Laser power is reduced to avoid heating the samples, using optical filters of various optical densities, and was always lower than 5 mW. The acquisition time is 15 seconds, with each measurement repeated 6 times. 10 to 15 spectra are recorded for each sample for statistical

purposes. Peak fitting is performed using the Peak Analyser of the OriginPro 8.5.1 software. The following expression (Beyssac *et al.*, 2002) is used to derive peak temperature conditions: T(°C)= –445R2 + 641, with R2 (peak area ratio) = (D1/(G+D1+D2)).

3.3. Stable isotopes

3.3.1 $\delta^{18}O$ and $\delta^{13}C$ of siderite

15 to 20 mg of siderite were reacted at 70 °C with H_3PO_4 for 15 days (Scheppard & Schwarcz, 1970). Isotopic ratios were measured using a modified VG 602D mass spectrometer at the CRPG laboratory (Vandœuvre-lès-Nancy, France), and the results are reported using conventional $\delta^{18}O$ (V-SMOW) and $\delta^{13}C$ (V-PDB) notations. The analytical reproducibility is ±0.1 ‰ for $\delta^{18}O$ and $\delta^{13}C$.

3.3.2 $\delta^{18}O$ of quartz

6.5 to 7.5 mg of quartz (same grains as those used for fluid inclusion analyses) were analysed using the conventional fluorination method (Clayton & Mayeda, (1963). The measurements were carried out with a VG SIRA 10 triple-collector instrument at the University of Rennes 1 (France). The analytical reproducibility (estimated from duplicates performed on different Ni fluorination tubes) is ±0.2‰.

3.3.3 $\delta^{34}S$ of sulphides and sulphates

Sulphur isotope compositions were measured following the method of Giesemann *et al.* (1994) at the CRPG laboratory (Vandœuvre-lès-Nancy, France) by EA-IRMS (Elemental Analyser-Isotopic Ratio Mass Spectrometer). $\delta^{34}S$ was measured with a GV Instruments Isoprime mass spectrometer coupled in continuous-flow mode to a EuroVector elemental analyser. Results are reported using conventional $\delta^{34}S$ (CDT). No inter-sample memory effect was observed. Linearity of the mass spectrometer and reproducibility of the analysis were checked using CRPG internal reference materials. The analytical reproducibility obtained on the barium sulphate reference material used at CRPG is lower than 0.3 ‰.

3.3.4 δD of white micas

2 to 3 mg of powdered host-rock were analysed for the isotopic composition of hydrogen-bearing minerals, mainly phengite. δD was measured with a GV Instruments Isoprime mass spectrometer coupled in continuous-flow mode to a EuroVector elemental analyser. No inter-sample memory effect can be observed. Linearity of the mass spectrometer and reproducibility of the analysis were checked using CRPG internal reference materials with an analytical reproducibility lower than 0.3‰.

3.3.5 δD of fluid inclusions

Fluids trapped in quartz, barite and siderite crystals were extracted for isotopic analyses by crushing under vacuum. Aliquots of 1.0 to 5.1 g of mn-sized grains were loaded into steel tubes and degassed overnight at 120 °C under vacuum to release any water adsorbed at the mineral surface (Dublyansky & Spötl, 2009). Preliminary tests conducted under the microthermometric heating stage showed no decrepitation or stretching of the studied fluid inclusions at temperatures below 200 °C. H_2O was separated cryogenically from other gases and reduced to H_2 in a uranium reactor at 800 °C. D/H ratio of H_2 was determined using a dual–inlet VG Micromass 602D mass spectrometer at the CRPG laboratory (Vandœuvre-lès-Nancy, France). External reproducibility of D/H measurements was estimated to be lower than 3 ‰ by normalizing raw data to the V-SMOW-SLAP scale. Two CRPG water standards were analysed along with each weekly batch of water samples obtained from the fluid inclusions.

To avoid any memory effect on D/H ratios within the uranium reactor, samples were systematically duplicated. For each duplicate, δD values from the first extraction are discarded since they could be affected by this memory effect.

For quartz containing primary inclusions, $\delta^{18}O_{fluid}$ was calculated from $\delta^{18}O_{quartz}$ using the quartz-water fractionation equation of Zheng (1993) at a given temperature.

4. Results

4.1. Characteristics of the host-rock

All sampled veins are hosted in schists composed of phengite, quartz, graphite and rutile. Although not observed in this study, biotite and garnet have also been described in these rocks (Álvarez & Aldaya, 1985) as well as chloritoid (Booth-Rea *et al.*, 2004). The strike of the foliation on the western flank of Sierra Almagrera (the studied area) oscillates between N045E and N100E, with an average dip of around 25-30ºSE-S that can reach up to 45ºSE-S at El Arteal mine (Figure 1-b). Although stretching lineation is not always observed, deformed quartz veins (V-Qtz1) indicate a top to the West shearing (Figure 2-a).

The Raman study of graphitic carbon yields R2 ratios from 0.12 to 0.21 (mode: 0.18; n=8, in 3 samples), corresponding to temperatures ranging between 545 and 590 °C. These results are in agreement with the temperatures of 535-550 °C determined using the same method in the Calar Alto unit from the Sierra de Los Filabres (Augier *et al.*, 2005b). Phengite shows Si contents ranging from 3.31 to 3.05 a.p.f.u (n=4, in 2 samples), corresponding to an estimated pressure ranging from 2.2 kbar at 545 °C to 9.7 kbar at 590 °C (Massonne & Schreyer, 1987). These pressures are similar to those obtained in the Calar-Alto unit in the Sierra de Los Filabres (10±0.7 kbar to 3.1±0.3 kbar) (Augier *et al.*, 2005b).

4.2. Vein and fluid inclusion petrography

According to their geometry, petrography and position relative to the host rock foliation, five types of veins can be defined (Table 2). Table 3 summarizes the characteristics of the fluid inclusions observed within each vein.

4.2.1 V-Qtz1, quartz veins parallel to host-rock foliation

V-Qtz1 veins (thickness less than 30 cm) may be found in both structural blocks (Figure 2-a). These quartz veins are characterised by high-temperature recrystallization mechanisms with granoblastic euhedral texture, with grains of about 200 μm showing triple points with an angle of

120° (Figure 2-b) or lobate grain boundaries interpreted as due to grain boundary migration (Jessell, 1987, Passchier & Trouw, 2005, Stipp & Kunze, 2008) (Figure 2-c). No primary inclusions are observed in Qtz1 grains, and transgranular fluid inclusion planes are only observed in the Sierra Almagrera mining district. Relative chronology criteria indicate that Qtz1-tg1 predates Qtz1-tg2. Each set of plane displays a distinct orientation (Figure 2-d-e-f; Table 3).

4.2.2 V-Qtz2, quartz veins parallel to or oblique to host-rock foliation

V-Qtz2 (thickness of about 10 cm) are oblique to the rock foliation along certain sections of the vein, while other parts are parallel (Figure 3-a). Since V-Qtz2 partly crosscuts the rock foliation, they are considered as postdating V-Qtz1, which is parallel to the foliation. V-Qtz2 are characterized by anhedral quartz grains of about 3-5 mm, showing undulose extinction. These grains are characterized by wave-shaped grain-boundaries and subgrain boundaries. Subgrain rotation and bulging recrystallization processes can be distinguished (Figure 3-b). Microstructures indicate dynamic recrystallization processes at slightly lower temperatures than V-Qtz1 (Figure 3-b; Passchier & Trouw, (2005)). Fluid inclusions in V-Qtz2 are found within intragranular (Qtz2-ig) (Figure 3-b-c) or transgranular planes (Qtz2-tg) (Figure 4-a-b-e). The direction and dip of Qtz2-ig fluid inclusion planes are randomly distributed (Figure 3-e) throughout the vein, but are parallel to each other within a single grain. This suggests that these veins are related to crystallographic directions reactivated during crystal plastic deformation rather than tectonic fracturing. Qtz2-tg veins are parallel to each other and to the walls of V-Qtz2 (Figure 4-b-e). They were likely produced by crack-and-seal deformation.

4.2.3 V-Qtz3, oblique veins from the mining district

V-Qtz3 are composed of euhedral quartz associated with hematite, developed in veins (thickness < 5 cm) oblique to the host-rock foliation or in voids. Although euhedral Qtz3 overgrows Qtz2 (Figure 4-b), it is never intersected by Qtz2-tg. Isolated primary fluid inclusions are interpreted as contemporaneous to crystal growth (Qtz3-p; Figure 4-f). Hematite is found within microfissures extending from the wall rock to Qtz2 (Figure 4-b-d) and in voids between euhedral

Qtz3 (Figure 4-a-b). The lack of microfractures affecting Qtz3 and the almost systematic association of Qtz3 with hematite minerals suggest that both minerals grew during the same mineralization event.

4.2.4 V-ore, oblique mineralised veins from the mining district

An extensive study of ore mineralogy in the mining district (Morales Ruano, 1994) shows the occurrence of abundant siderite, barite, pyrite, marcasite, galena, chalcopyrite, sphalerite, tetrahedrite-tennantite, veenite, gersdorffite and bournonite and trace amounts of pyrrothite, bismuthinite, arsenopyrite and bravoite. Our sampled veins (V-ore) show only part of this paragenesis.

V-ore veins crosscut V-Qtz1 (Figure 5-a), V-Qtz2 and V-Qtz3 (Figure 4-a). The thickness of the sampled V-ore veins can reach several dm. They are distributed in two main clusters striking N000-160E and N120-130E. Micro-euhedral quartz (0.5-1.0 mm) is observed on the walls of V-ore (Figure 5-a) predating siderite formation. Pyrite is included in siderite (Figure 5-c). Galena occurs at the contact between siderite and barite (Figure 5-b). The mineral sequence can be summarized as follows: micro-euhedral quartz-siderite-pyrite-galena-barite (Figure 5-c).

Qtz-ore-tg inclusions are parallel to the wall rock and crosscut several micro-euhedral quartz grains. Fluid inclusions in siderite and barite are observed along cleavage planes and interpreted as primary (Figure 5-d-e).

4.2.5 V-Cal, oblique calcite veins from the subsident area

These lenticular tension gashes crosscut V-Qtz2 and attain a length of several cm with an opening of a few mm (Figure 6-a). Fluid inclusions are found as clusters and are interpreted as primary (Figure 6-b-c).

4.3. Microthermometry and Raman results

Table 3 presents data concerning the size, shape and filling of the fluid inclusions. The characteristic phase-transition temperatures and calculated compositions of fluid inclusions are

reported in Table 4 and Figure 7. Aqueous carbonic fluid inclusions are recorded in quartz veins (Qtz1-tg1, tg2, Qtz2-ig, Qtz2-tg and Qtz3-tg), whereas aqueous fluid inclusions are recorded in ore veins.

4.3.1 Fluid inclusions in Qtz1

The salinity of Qtz1-tg1 ranges between 9.7 and 22.6 mass% $NaCl_{eq.}$, with T_h (L) between 319 and 350 °C. The volatile phase is predominantly CO_2 (70-85 vol%), with minor amounts of CH_4 (10-17 vol %) and N_2 (0-18 vol%).

The salinity of Qtz1-tg2 ranges between 21.6 and 23.8 mass% $NaCl_{eq}$, with T_h (L) between 305 and 344 °C. The volatile phase is predominantly CO_2 (89-97 vol %), with minor amounts of CH_4 (0-8 vol%) and N_2 (0-7 vol%).

4.3.2 Fluid inclusions in Qtz2

The salinity of Qtz2-ig ranges between 11.9 and 20.6 mass% $NaCl_{eq.}$, with T_h (L) between 220 and 400 °C. This broad scatter of homogenization temperatures is attributed to volume modification of fluid inclusions during high-temperature deformation (Vityk *et al.*, 1995, Bodnar, 2003, Diamond *et al.*, 2010). Therefore, we only consider T_h of intact inclusions with the smallest gas bubbles (flw > 65 vol %), resulting in a range from 220 to 355 °C. The volatile phase is dominated by CO_2 (87-98 vol %), with minor amounts of CH_4 (1-8 vol %) and N_2 (1-7 vol %).

The salinity of Qtz2-tg ranges between 0.1 and 2.4 mass% $NaCl_{eq.}$, with T_h (L) between 290 and 330 °C. Raman spectroscopy shows that the volatile phase is predominantly CO_2 (57-85 vol %), with presence of CH_4 (5-30 vol %), N_2 (7-12 vol %) and H_2S (1-5 vol %).

4.3.3 Fluid inclusions in Qtz3

The salinity of Qtz3-p ranges between 12.7 and 20.9 mass% $NaCl_{eq.}$, with T_h (L) between 235 and 310 °C. The volatile phase is predominantly CO_2 (91-99 vol %), with minor amounts of CH_4 (1-7 vol %) and N_2 (0-5 vol %).

4.3.4 Fluid inclusions in Qtz, Sd and Brt from V-ore veins

The salinity of Qtz-ore-tg ranges between 18.4 and 25.0 mass% $NaCl_{eq.}$. Methane (traces) is the only volatile present. T_h(L) ranges between 150 and 248 °C.

The salinity of Sd-p ranges between 15.4 and 24.6 mass% $NaCl_{eq.}$. Because no hydrohalite melting or clathrate dissociation temperature could be observed, our calculation is based on the final ice melting only and does not take into account the complexity of the fluid system. Therefore, some data yield salinity higher than halite saturation in the H_2O-NaCl system. T_h (L) is observed between 110 and 222 °C. Such a large variation is likely related to leakage within this highly cleavable mineral (Bodnar, 2003). Raman spectroscopy shows that CH_4 is the only volatile in the gas phase.

The salinity of Brt-p ranges between 20.7 and 25.8 mass% $NaCl_{eq.}$. Again, because hydrohalite is never observed, our calculations only take account of T_m(ice) and the complexity of the system is not fully expressed. Therefore, some of our data show salinities higher than NaCl saturation in the H_2O-NaCl system. T_h (L) is observed between 237 and 335 °C. Although the inclusions were carefully checked before and after measurements, leakage before microthermometric experiments cannot be excluded (Ulrich & Bodnar, 1988, Bodnar, 2003), so these values in barite should be considered very carefully. Raman spectroscopy shows that the volatile phase is predominantly composed of CO_2 (45-93 vol %) (although present in small amount) and N_2 (5-52 vol %) with minor CH_4 (0-5 vol %).

4.3.5 Fluid inclusions in calcite from V-Cal

The salinity of Cal-p ranges between 11.8 and 18.4 mass% $NaCl_{eq.}$, with T_h (L) between 67 and 87 °C (Figure 7). Raman spectroscopy does not allow us to identify the nature of the gas phase.

4.4. Halogen chemistry

For V-Qtz1, a Cl/Br molar ratio of 1000 is obtained by crush-leach analysis and LA-ICPMS for a chlorinity of 4200 mmol/kg solution (Figure 8). The crushing experiments release fluids derived from Qtz1-tg1 and Qtz1-tg2 as well as the fluid contained at grain boundaries.

Sd-p and Brt-p yield a Cl/Br ratio of between 3 500 and 10 000 for a chlorinity between 4 200 and 5 400 mmol/kg solution, respectively. The Cl/Br ratio of Brt-p obtained with LA-ICP-MS is between 1 200 and 4 500 (Figure 8). The other populations of fluid did not give an interpretable signal.

4.5. Major and trace element chemistry

In both types of fluids (Qtz1-tg1 (n=8), Qtz2-tg (n=2), Qtz3-p (n=4) and Brt-p (n=9)) inclusions major (Na, K, Mg) and trace elements (Li, Mn, Fe, Cu, Zn, Sr and Ba) have been measured (Table 5, Figure 9). The other generations of fluids do not give any interpretable signals.

In Qtz1-tg1 high salinity fluid, Na content ranges from 27000 to 122 000 ppm, K from 2000 to 7600 ppm, yielding Na/K ratio ranging from 10 to 30. Mg content is relatively variable (100-1600ppm). Li content is relatively high (200 to 1000 ppm). Mn, Fe, Ba and Sr display noticeable concentration (Table 5, Figure 9).

On the contrary, Qtz2-tg having very low salinity show lower cation content and Na/K ratio is ranging from 1 to 6. Due to the low salinity fluid, few data could be obtained.

Qtz3-p fluids displayed similar values as for Qtz1-tg1 (Na around 70 000 ppm). However K content is lower (1500 ppm) and consequently Na/K ratio is higher (around 50). Mg, Sr, and Mn content are the highest (Table 5, Figure 9).

In Brt-p fluids, Ba and Sr content could not be measured due to matrix contamination. Na content is slightly lower than those of Qtz1-tg1 (20000 and 65000 ppm) wheras K content is ranging from 2600 and 9500 ppm (Na/K: 4 to 10). It can be notice that Zn content could reach 4700 ppm. However, we cannot exclude a contribution of the barite crystal (Table 5, Figure 9).

4.6. Stable isotopes

$\delta^{13}C$ in siderite ranges between –9.5 and –10.9 ‰ $_{V\text{-}PDB}$ (n=4), while $\delta^{18}O$ ranges between 20.6 and 22.5 ‰ $_{V\text{-}SMOW}$ (Table 6). $\delta^{18}O$ in barite ranges from 13.0 to 13.2 ‰ $_{V\text{-}SMOW}$ (n=2), and δ34S (n=4) from 19.4 to 23.1‰ $_{V\text{-}CDT}$. Pyrite (n=3) yields $\delta^{34}S$ between 5.4 and 6.4 ‰ $_{V\text{-}CDT}$ and galena (n=3) yields $\delta^{34}S$ between –2.4 and 8.3 ‰ $_{V\text{-}CDT}$.

Table 6 reports the $\delta^{18}O$ values of minerals containing fluid inclusions. White micas from the host-rock yield δD values of –52 ± 1 ‰ $_{V\text{-}SMOW}$. δD_{fluid} values from Qtz1 sampled in the subsident area (recrystallised quartz devoid of visible inclusions) range between –33 and –36 ‰ $_{V\text{-}SMOW}$. Former trapped fluid inclusions appear to have been transported to the grain boundaries during hydrolytic weakening (e.g. (Kerrich, 1976, Wilkins & Barkas, 1978, Johnson & Hollister, 1995, Hollister, 1990, Bakker & Jansen, 1990, 1994), so it is likely that remnants of this fluid were measured. In the mining district, V-Qtz1 veins host Qtz1-tg1 and Qtz1-tg2 type inclusions. The transgranular fluid inclusion planes show δD values between –28 and –32 ‰ $_{V\text{-}SMOW}$, possibly reflecting the influence of δD inherited from earlier fluids displaced to grain boundaries during quartz recrystallization.

δD_{fluid} from Qtz2-ig and Qtz3-p inclusions cover a similar range between –23 and –36 ‰ $_{V\text{-}SMOW}$ (Table 6, Figure 10). δD_{fluid} from Qtz2-tg (selected section with dominant Qtz2-tg inclusions in the quartz grains) display a larger range of values between –17 and –48 ‰ $_{V\text{-}SMOW}$ (Table 6, Figure 10).

V-ore veins are significantly more D-depleted. δD_{fluid} of Sd-p range between –65 and –80 ‰ V-SMOW. δD_{fluid} of Brt-p ranges between –53 and –69 ‰ $_{V\text{-}SMOW}$ (Table 6, Figure 10).

5. Discussion

5.1. Key criteria to reconstruct the fluid sequence

Early fluid stage: Ductile deformation affecting V-Qtz1 and V-Qtz2 in the Sierra Almagrera is compatible with top-to-the-W / top-to-the-SW extensional shearing similar to that observed in the Sierra de los Filabres (Augier *et al.*, 2005c) (Figure 1). This deformation is not dated in the Sierra Almagrera. The only known age constraint is given by the youngest ductile extensional stages recognized within the Betics metamorphic pile, which are dated around the Langhian-Serravalian boundary at 14 Ma (Gomez-Pugnaire et al., 2004, Platt et al., 2006, Gomez-Pugnaire et al., 2012).

Although no fluid inclusions are observed in V-Qtz1 veins sampled from the subsident area, crushing techniques allowed us to extract a fluid, which could then be analysed for its δD. This

suggests that fluid inclusions trapped prior to plastic deformation are displaced towards grain boundaries during recrystallization processes (Kerrich, 1976, Wilkins & Barkas, 1978, Johnson & Hollister, 1995) and are then partly preserved. The calculated equilibrium temperature between this fluid and host-rock, based on hydrogen isotope fractionation, is comprised between 488 and 520 °C (Table 6), which is in agreement with ductile conditions. Plastically deformed or dismembered inclusions are found within intragranular planes of V-Qtz2 (Qtz2-ig), while non-deformed inclusions are found within transgranular planes affecting V-Qtz1 in the mining district where V-ore barite veins are also frequently present. Transgranular planes result from the healing of former open cracks (Lespinasse, 1999, Lespinasse et al., 2005), and thus more brittle conditions are required than for intragranular planes. As a consequence, Qtz2-ig likely formed at conditions more ductile than Qtz1-tg1, 2.

Similar microthermometric phase transitions are observed for Qtz2-ig and Qtz1-tg1, 2 (average T_h around 340 °C and with comparable maximum salinity). Relative chronology criteria indicate that Qtz1-tg1 predates Qtz1-tg2, but no other direct data allow us to constrain the chronological position of Qtz1-tg (1, 2) in the general fluid history. Two interpretations can be proposed. The dominant NW-SE strike of Qtz1-tg1 may be consistent with late Tortonian shortening directions associated with strike-slip tectonics (Montenat & Ott D'estevou, 1990). This deformation occurred prior to the Messinian N-S to NNE-SSW shortening that could correspond to the subsequent Qtz1-tg2 fluid inclusion planes. In such a scenario, the transgranular fluid inclusions could be coeval with V-ore mineralizing events displaying similar tectonic directions, and thus would not correspond to an early fluid trapped during the brittle-ductile transition.

An alternative explanation would be that both kinds of microcracks are related to brittle extensional fracturing, implying that the tectonic regime previously expressed by ductile deformation belongs to an earlier stage of exhumation. In such a case, the brittle deformation would predate the onset of a Late Miocene transcurrent regime related to the mineralizing events. Therefore, σ3 measured normal to the microcracks would be similar for both the extensional and

transcurrent regimes, with the result that this question cannot be resolved solely on the basis of structural criteria. If fluids were trapped soon after the ductile-brittle transition for quartz, this would explain certain similarities of the microthermometry and salinity data with Qtz2-ig fluid inclusions trapped during this transition.

Intermediate fluid stage: Qtz2-tg fluids are characterised by a much lower salinity than observed in the other types of fluid inclusions. Since Qtz2-tg never affects V-Qtz3 nor V-Cal, this suggests an episodic arrival of low-salinity fluid after the formation of V-Qtz2 but prior to V-Qtz3 and V-Cal. Considering the youngest ages inferred for ductile deformation in the eastern Betics (around the Langhian-Serravalian boundary), the exhumation of this part of the Sierra Almagrera within the brittle domain probably occurred during Langhian to Serravalian times. Only marine sediments of Serravalian age are preserved further north in the Aguilas block (Griveaud *et al.*, 1990). Younger sediments of Late Serravalian – Early Tortonian age recognized further west in the Huercal Overa Basin (Pedrera *et al.*, 2010) are represented by alluvial fan deposits reflecting the uplift of mountain ranges prior to the return of marine conditions in the Vera Basin from Late Tortonian times onwards (Figure 1). The uplift of the Sierra de los Filabres bordering the Huercal Overa Basin has been linked to a local N-S extension (Augier *et al.*, 2005a) or the onset of transcurrent tectonics (Montenat & Ott D'estevou, 1990). Regardless of the associated tectonic regime at this time, the paleogeography suggests that hydrogeological conditions within the brittle crust favoured the input of meteoric water from the uplifted ranges into the upper reservoir, but prior to the Late Tortonian return to marine conditions.

Pre-ore fluid stage: The obliquity with respect to the host-rock foliation and the lack of undulose extinction in the euhedral quartz shows that V-Qtz3 formed within the brittle domain. Euhedral Qtz3 formed during the same event that led to the formation of hematite. The input of Fe in the fluid is related here to an increase of salinity. Although oxidizing conditions prevailed at a certain stage of the fluid evolution, it is possible that early siderite was subsequently oxidized.

Ore fluid stage: V-ore veins crosscut V-Qtz3 (Figure 4-a). The maximum salinities are observed either in fluid inclusions from transgranular planes within early micro-euhedral quartz on the wall-rock (Qtz-ore-tg), or in primary fluid inclusions from siderite and barite (Sd-p and Brt-p). The formation of siderite postdating V-Qtz3-hematite veins not only indicates the ongoing input of Fe in the fluid, but also a shift towards reducing conditions. Quartz and siderite trapped fluids at lower temperatures (T_h of Sd-p around 190 °C) compared with the pre-ore fluid stage (T_h of Qtz3-p around 265 °C). V-ore vein sets have two main strike directions: N000E-N340E and N120E-N130E. The N-S trend is coherent with the Messinian direction of horizontal shortening and E-W extension, being related to the major transcurrent activity of the Palomares Fault Zone. The interpretation of fluid inclusions in barite is more problematic. The data appears to indicate an increase of T_h compared to the estimated conditions of siderite formation (Figure 7), but T_h obtained from this kind of mineral are usually considered to be overestimated (Ulrich & Bodnar, 1988). This raises the question of the chronological position of N-S to NNE-SSW-striking fluid inclusion planes belonging to Qtz1-tg2, since both Brt-p and Qtz1-tg2 show closely similar Th values and high salinities (Figure 7). It is possible that this similarity is just a coincidence or maybe Qtz1-tg2 inclusions in quartz reflect a thermal pulse that leads to values typical of Brt-p.

Late fluid stage: Inclusions in calcite record lower T_h around 80 ºC, suggesting formation at a more superficial position. The relative chronology of this late stage in the fluid sequence could be debated since the calcite veins were not sampled in the same structural block as V-ore veins. The only chronological criterion is the crosscutting geometry with V-Qtz2.

5.2. *P-V-T-X evolution*

The Raman spectrometry study of graphitic schists constrains the maximum temperature attained by the host-rock to 545-587 °C. These results are in agreement with metamorphic peak temperatures of the Nevado-Filábride complex obtained in other parts of the orogen (De Jong, 2003, Augier *et al.*, 2005b).

The *P-T* ranges of fluid inclusion entrapment are constrained by the isochores and geothermal gradients (Figure 11). For the Sierra Almagrera, geothermal gradient data are poorly documented. The only available data comes from the Sierra Nevada located to the West of Sierra Almagrera, where a gradient of 60 °C/km under lithostatic conditions is indicated for the final stages during ductile deformation (Gomez-Pugnaire & Fernandez-Soler, 1987, Bakker *et al.*, 1989, Jabaloy *et al.*, 1993, Augier *et al.*, 2005b). A gradient of 30 °C/km is arbitrarily taken as an upper limit, corresponding to the European average anorogenic gradient.

In the absence of other metamorphic constraints, hydrogen isotopes can be used to assess the temperature of equilibrium between fluid inclusions and mica-rich host-rock (Tarantola *et al.*, 2007). In the case of isotopic equilibrium, *P- T* boxes are also constrained by the minimum and maximum values of hydrogen equilibrium temperatures (Table 6 and Figure 11).

Early fluid stage: Qtz2-ig inclusion shapes range from euhedral to dismembered (Tarantola *et al.*, 2010 and 2012), with large variations of the gas filling ratio. This is indicative of plastic deformation and would thus be related to lithostatic pressure conditions. The box shown in Figure 11 is also constrained by minimum and maximum hydrogen equilibrium temperatures since the calculated temperatures are of the order of 400-520 °C (Table 6).

Transgranular fluid inclusion planes Qtz1-tg1 and Qtz1-tg2 indicate brittle behaviour within the quartz vein, but the mica-rich host-rock may still have been affected by ductile deformation. Fluids may have been trapped during the brittle-ductile transition of mica-rich lithologies within a temperature and pressure range already corresponding to brittle rheology for the quartz. In such a case, both Qtz1-tg1 and Qtz1-tg2 possibly formed under a lithostatic regime. As an alternative hypothesis, these microcracks may be indicative of a hydrostatic regime due to late Miocene transcurrent tectonics that formed V-ore veins in the brittle domain. In fact, Qtz1-tg1/Qtz1-tg2 fluids seem to be in equilibrium with the host-rock (Table 6), but in strong disequilibrium with respect to V-ore veins. In addition, the gas contents of Qtz1-tg1 and Qtz1-tg2 are more closely similar than those of Sd-p and Brt-p fluid inclusions (Table 4). All these data suggest a resident

fluid derived from the lower reservoir rather than the presence of fluids of external origin in the upper reservoir. Finally, this explains why Qtz1-tg1 and Qtz1-tg2 could be related to the early fluid stage in the selected scenario (Figure 11). Thus, the rather large *T* and *P* range reflects the trapping conditions of inclusions related to this stage between Qtz2-ig (400-520 °C and 270-380 MPa) and Qtz1-tg1, 2 (440-480 °C and 110-230 MPa) (Figure 11).

Intermediate fluid stage: There is no evidence of whether transgranular Qtz2-tg planes formed under a lithostatic or a hydrostatic fluid regime. From this intermediate stage of fluid evolution until the final stages of fluid trapping, the hydrogen isotope fractionation seems to be no longer in equilibrium between the fluid inclusions and the mica-rich host-rock (Table 6). Hydrogen equilibrium temperature constraints do not allow us to define the *P-V-T-X* boxes. The decrease of salinity related to an input of surficial fluids rather suggests an opening of the system under hydrostatic conditions. The trapping conditions for these fluid inclusions are in the range 300-450 °C and 40-140 MPa (Figure 11).

Pre-ore fluid stage: Since the euhedral quartz Qtz3 veins were no longer affected by ductile deformation and recrystallization processes, it is considered that they crystallized in the brittle domain under hydrostatic pressure, within the *P-T* range: 250-380 °C and 40-120 MPa (Figure 11).

Ore fluid stage: Crystallization of quartz, siderite and barite occurred in an open system. Hydrostatic conditions allow us to constrain the *P-T* range of entrapment for fluid inclusions at 160-300 °C and 30-90 MPa in Qtz-ore-tg and at 120-260 °C and 20-80 MPa in Sd-p (Figure 11). Unfortunately, the confidence on microthermometric data obtained on barite is low (Ulrich & Bodnar, 1988). The observed homogenization temperatures would imply a significant increase of the trapping temperature to 280-440 °C at 40-130 MPa. This could be explained by a magmatic input from contemporaneous active volcanism, but it could also be related to an overestimation due to stretched inclusions in barite. T_h and salinity of Brt-p are similar to Qtz1-tg2 inclusions, while strike directions of barite V-ore veins are more or less parallel to Qtz1-tg2 fluid inclusion planes. These inclusions in quartz support the hypothesis of a thermal pulse defined by inclusions in barite.

In fact, *P-V-T-X* data from Qtz1-tg2 (Figure 11) seem to indicate a significant increase of pressure compared to Sd-p fluid trapping conditions, which is apparently incompatible with an ongoing exhumation of the Sierra Almagrera. Hydrogen isotopic fractionation indicates a strong disequilibrium between primary fluid inclusions from V-ore veins and the host-rock. On the contrary, hydrogen isotope data for Qtz1-tg2 indicate a fluid in equilibrium, rather suggesting its formation during an early fluid stage. This interpretation does not support the existence of a thermal pulse.

Late fluid stage: The calcite stage is characterized by lower homogenization temperatures, suggesting a cooling of the system down to 70-110 °C at 10-30 MPa hydrostatic pressure (Figure 11).

5.3. Source of fluids

Early fluid stage: Hydrogen isotope fractionation data showing equilibrium between fluid inclusions and mica-rich host-rock suggest a resident fluid in the lower reservoir. The δD_{fluid} values obtained from Qtz1 (early fluids displaced towards grain boundaries during recrystallization processes) and Qtz2-ig ranging between –23 and –36 ‰ $_{V\text{-}SMOW}$ (Table 6, Figure 10) are compatible with a fluid of metamorphic origin.

V-Qtz1 quartz grains also containing Qtz1-tg1 and Qtz1-tg2 fluids yield similar *δD* values (–28 to –30 ‰ $_{V\text{-}SMOW}$). Their halogen signatures plot along the seawater evaporation trend in agreement with halite evaporation (Figure 8). At first sight, this would indicate a primary brine. Two brine sources can be considered according to the geological history: Triassic and Messinian. It is very unlikely that primary brines could have been preserved since Triassic times, considering the metamorphic processes affecting the rocks in the lower reservoir. The other hypothesis would be to explain Qtz1-tg1 and Qtz1-tg2 signatures as representing surficial brines coming from Messinian pre-crisis evaporitic basins. This interpretation revives the hypothesis linking Qtz1-tg2 and Brt-p inclusions during mineralization events. However, stable isotope results and *P-V-T-X* data rather identify fluids trapped in Qtz1-tg1 and Qtz1-tg2 microcracks as resident fluids that have undergone

long-time fluid-rock exchange with the mica-rich host-rock. The interaction of fluids with black graphite schists may have led to a Br enrichment (Yardley, 2005) of secondary brines derived from the dissolution of Triassic evaporites, which could explain the position of the data points on the seawater evaporation curve (Figure 8).

The variability observed in the salinity of both Qtz2-ig and Qtz1-tg1/Qtz1-tg2 fluids might either reflect i) an original heterogeneity related to discontinuous interaction with Permo-Triassic evaporites, ii) the effect of plastic deformation for Qtz2-ig (Diamond *et al.*, 2010), or iii) a mixing between deep high-salinity and a low-salinity fluid end-members.

Intermediate fluid stage: Fluid isotope values obtained on Qtz2 grains containing Qtz2-tg also incorporate the signature of fluids from the early stage displaced to grain boundaries during recrystallization processes. δD_{fluid} values ranging from –17 to –48 ‰ $_{V\text{-}SMOW}$ are generally lower than values obtained for the early fluid stage. δD values of the dilute fluid are thus D-depleted compared to those of the early stage, with values that are unlikely to be buffered by the host-rock (Table 6). This suggests the input of an external low-salinity fluid from the upper reservoir, which did not interact with evaporites/metaevaporites (i.e. Permo-Triassic).

It is possible that the volume of low-salinity fluids was sufficient to dilute high-salinity fluids from the early stage, or more likely, the lower ductile and the upper brittle reservoirs were not connected during exhumation and thus behaved independently. The penetration of low-salinity fluids is likely associated with the uplift of mountain ranges during the Serravalian and Early Tortonian (Martínez-Martínez & Azañón, 2002, Platt, 2007) (Figure 12). However, in the absence of $\delta^{18}O$ values and interpretable LA-ICP-MS data, it cannot be concluded whether this fluid is of meteoric or basinal origin.

Pre-ore fluid stage: Hydrogen isotopic composition is not buffered by the host-rock (Table 6). The enrichment of iron in the fluid led also to the formation of hematite in the voids between Qtz3 crystals (Figure 4-b and Figure 12). This stage corresponds to tectonic conditions in the brittle domain.

The salinity is comparable to that in the early fluid stage. $\delta^{18}O_{quartz}$ is lower than for the early fluid stage, and trapping temperatures define a $\delta D/\delta^{18}O_{fluid}$ signature shifted towards basinal/meteoric water compositions. The major and trace elements (Na/K ratio around 50, Sr/Ba ratio around 20 and Sr, Mg content, Table 5) of this fluid reflect a basinal origin (Yardley, 2005). These data are coherent with mixing between low-salinity basinal/meteoric fluids and with an upward migration of high-salinity fluids coming from the lower reservoir. This may reflect the onset of transcurrent tectonics during this period, and a structural connection between the two reservoirs through the brittle ductile transition zone (Figure 12).

Ore fluid stage: Although siderite from El Arteal in the mining district yields slightly lower $\delta^{13}C$ (about 2 ‰, with values of –9.5 and –10.9 ‰ $_{V\text{-}PDB}$) and slightly higher $\delta^{18}O$ (about 1 ‰ $_{V\text{-}SMOW}$), it can be compared with the siderite from Jaroso Ravine (Figure 1-b). The results from this latter locality have been interpreted as indicative of meteoric water and low-temperature hydrothermal conditions (Martinez-Frias *et al.*, 2007). However, $\delta^{13}C$ may also be buffered by the metasedimentary sequence during fluid interaction, whatever the origin of the fluids.

The combination of δD and $\delta^{18}O$ values suggests a fluid with a magmatic or metamorphic signature (Field & Fifarek, 1985). As well as having a high salinity, the fluids do not fit the meteoric water line (Figure 10), thus contradicting the conclusions of Martinez-Frias *et al.* (2007). Since δD_{fluid} is strongly in disequilibrium with the host-rock, this implies an external source for the ore fluid, so it cannot be of meteoric origin.

Fluids in siderite were trapped at lower temperatures than the previous fluid stages, and thus at shallower depths (Figure 12). The fluid inclusions in siderite show higher values of salinity than obtained for the earlier stages, reaching up to 25 mass% $NaCl_{eq.}$ (Figure 7, Table 4). Cl/Br data show that the fluid is Br-depleted and far from the seawater evaporation trend. As Br is not easily incorporated in halite, dissolution of halite would yield this type of fluid. Cl/Br ratios thus indicate signatures that could be compared to secondary brines (Banks *et al.*, 2000) resulting from dissolution of evaporites (Figure 8).

The strong salinity increase might result from a combination of volcanism in the Palomares Fault Zone, as suggested by δD and $\delta^{18}O$ values (Figure 10), and dissolution of evaporites as suggested by their halogen signatures (Figure 8). The strike direction of the veins is coherent with the Messinian strike-slip regime related to major activity of the Palomares Fault Zone (Montenat *et al.*, 1987, Booth-Rea *et al.*, 2004). Of major interest here is the $\delta^{34}S$ composition of barite, which is more closely comparable to Miocene sea water (Claypool *et al.*, 1980, Morales Ruano *et al.*, 1995) than Triassic values. Therefore, the increase of salinity in the ore fluid stage compared to previous stages could also be related to secondary brines linked to the dissolution of Messinian evaporites rather than exclusively of Triassic evaporites. Dissolution of Messinian marginal evaporites (deposited from 5.96 to 5.67 Ma ago in the Sorbas basin) (Clauzon *et al.*, 1996, Bourillot *et al.*, 2009) is a possible scenario (Figure 12). These Messinian evaporites preceded the main sea-level drop related to the peak of the salinity crisis (5.60-5.46 Ma). Pre-incision Messinian evaporitic deposits were available, as revealed by the "Formation à blocs" in the Vera basin, which reworked Messinian early gypsum during the main incision event (Figure 12) (Clauzon, 1980, Clauzon *et al.*, 1996). Messinian sediments from Las Herrerias (Figure 1) were mineralised prior to the main Messinian incision (Alvado, 1986, Fortuin *et al.*, 1995, Booth-Rea *et al.*, 2004), and such a scenario would provide a relatively accurate dating of the mineralizing event around 5.65 Ma (Figure 12).

A thermal pulse at constant salinity is suspected because the fluid trapping conditions in barite exceed 400 ºC, but this result should rather be considered as an artefact arising from this particular mineral (Figure 12). If the high-K calc-alkaline, shoshonitic and ultrapotassic magmatism were related to mineralization during the ore-fluid stage, this could represent a possible metal source. The high contents of K or metals such Zn or Cu in fluid inclusions (Table 5, Figure 9) tend to support this hypothesis, but a leaching of basement rocks could also be an alternative explanation.

Late fluid stage: Homogenization temperatures of fluid inclusions within calcite around 80 ºC suggest deep burial or a shallow expression of hot fluids. The salinity of these fluids may be compared to the salinity of early and pre-ore stages. Calcite veins may correspond to a shallow

expression of deeper fluid flows, recorded as veins currently cropping out in the uplifted block represented by the mining district (Figure 12). In such a case, the superficial equivalent of rocks in the central block may have been eroded during the subsequent uplift, but preserved in the subsident block to the West. A second hypothesis is that these calcite veins only developed during a later stage at lower temperature.

Fluids trapped as fluid inclusion planes during the early stage are characterized by a rather low density of the CO_2-rich volatile phase. The significant presence of CH_4 (around 20% of the volatile molar composition) is not strictly expected in the case of water-graphite equilibrium (Dubessy, 1984, Huizenga, 2001, 2011). Such a distribution of volatiles is fairly common in metamorphic environments at around 350-450 °C, where local equilibrium is reached between water and graphite. Through mixing with other fluids, this contributes to the common metamorphic signature found in most retrograde fluids during exhumation (Cathelineau *et al.*, 1993, Boiron *et al.*, 2003). At lower temperatures, in the presence of graphite, CH_4 is expected to be the dominant species if redox conditions are moderately reducing. This applies in the case of a predominance of CH_4 in fluid inclusions during the precipitation of siderite at the beginning of the Ore stage, which occurred with a T_h around 190 °C. The precipitation of siderite from Fe^{2+}-rich solutions requires a significantly low fO_2 and an increase in fCO_2.

6. Conclusions

Fluid circulation events are recorded within the studied veins at different positions of the Sierra Almagrera metamorphic belt during its exhumation. The general *P-T* path is characterized by an evolution from lithostatic to hydrostatic conditions. Despite the rather exceptional constant fluid composition throughout exhumation, different geological contexts associated with fluid circulation can be considered: i) a first stage during which the host-rock passed through the brittle-ductile transition and the quartz trapped metamorphic fluids, ii) a second stage when the host-rock definitively entered the brittle domain and predominantly collected shallower fluids from the upper reservoir and, iii) a final stage, related to ore formation and possibly magmatism as well, resulting

in a marked tectonic change that modified the relative hydrogeologic independence between the deeper and upper reservoirs.

More generally, the tectonic and paleotopographic evolution of the Sierra Almagrera leads us to consider two stages in the fluid circulation history. Prior to the transcurrent tectonic regime, the metamorphic rocks of the Sierra Almagrera were exhumed as a whole, and V-Qtz1 and V-Qtz2 veins were developed throughout the studied area. The onset of transcurrent tectonics had two consequences: i) it localized the deformation and associated fluid pathways within the brittle crust and, ii) it generated local transtension and transpression leading to final exhumation of the central area corresponding to the mining district where V-Qtz3 and V-ore veins are found.

The first record of exhumation is characterized by ductile-brittle deformation related to extensional tectonics. We propose that, during this early stage, metamorphic brines resulted from the dissolution of Triassic evaporites. Low-salinity fluids were then recorded as the structural unit progressively entered the brittle domain. These low-salinity fluids are likely related to the penetration of basinal or meteoric waters from the surface, favoured by a hydraulic gradient related to the uplift of mountain ranges during late Serravalian to early Tortonian times.

The upper fluids could have retained their specific characteristics until the present-day, but the geodynamic changes related to the onset of Trans-Alboran tectono-volcanism modified the hydrogeological decoupling between the lower and upper reservoirs. The pre-ore stage is characterized by the occurrence of brittle quartz veins related to intermediate salinity and homogenization temperatures indicative of mixing between meteoric or basinal fluids and the upward migration of high-salinity fluids coming from the lower reservoir. These fluids are similar to those from the early fluid stage. They have a volatile phase dominated by CO_2 but devoid of CH_4, being associated with Fe which is expressed by the formation of hematite under oxidizing conditions, but possibly after the crystallization of primary siderite. This pre-ore stage can be interpreted as the first evidence of the influence of volcanism.

Reducing conditions prevailed at a later stage of Fe-rich fluid migration. This is reflected by the formation of siderite and Fe sulphides in the mining district, and is related to the activity of the Palomares sinistral fault zone during the Messinian. An evolution towards more oxidizing conditions led to the formation of galena and barite, whose $\delta^{34}S$ signatures indicate the involvement of Miocene sulphate. This suggests the involvement of a second type of secondary brines (Ore stage) which may have dissolved Messinian evaporites from the Vera Basin. Since the marginal evaporitic basins in the Betics are dated at around 5.96 to 5.67 Ma (Sorbas basin; Bourillot *et al.* (2009)), and since the Las Herrerias stratabound ore-deposits were incised during the main Messinian salinity crisis and sea-level fall in the Mediterranean domain (5.6-5.46 Ma), this scenario would provide an accurate constraint on the age of the mineralization stage around 5.65 Ma

The overall evolution of fluid migration in this part of the Betic Cordillera points out the role of three main driving forces: i) an exhumation path related to an overall cooling, ii) a drastic change to transcurrent tectonics associated with hydrogeological connections at depth favouring the ascent of hot hydrothermal fluids and, iii) the involvement of two types of secondary brines, an input from the deep reservoir involving Triassic evaporites and a more recent input from the Messinian at the surface, which might have caused the migration and concentration of elements of economic interest. The interference between these factors influenced the redox conditions within the upper brittle reservoir, leading to an alternation of oxidizing and reducing conditions that controlled the formation of Fe-rich minerals ((siderite?) hematite, then siderite-pyrite). The deep penetration of late-stage oxidizing Messinian secondary brines is related to the crystallization of barite. This process reflects the existence of large convection cells extending from the surface to deep aquifers, associated with transtensional tectonics and local heat flow, which are presumed to be related to Miocene magmatism at depth.

Acknowledgments

The authors thank M.-C. Caumon-Jodin (GeoRessources, Vandœuvre-lès-Nancy) for Raman spectroscopy analyses and T. Rigaudier (CRPG, Vandœuvre-lès-Nancy) for isotopic analyses. We

also thank A. Flammang and C. Demeurie who prepared thin and thick sections. Special thanks to C. Montenat for stimulating discussions on the geology and metallogeny of the Betic Cordillera. The authors also thank Michael Carpenter for his professional English language review. This work was supported by the Ministry of Higher Education and Research (MESR, France) and the CNRS ST-INSU-CT5 programme.

Alvado, J. C. (1986). Sédimentation, déformation et manifestation magmatiques associées au couloir de décrochement de Palomares : le bassin de Vera (SE de l'Espagne). Université de Paris.

Álvarez-Valero, A. M. & Kriegsman, L. M. (2008). Partial crustal melting beneath the Betic Cordillera (SE Spain): The case study of Mar Menor volcanic suite. *Lithos,* **101,** 379-396.

Álvarez, F. & Aldaya, F. (1985). Las unidades de la zona Bética en la región de Águilas-Mazarrón (Prov. de Murcia). *Estudios Geológicos,* **41(3),** 139-146.

Arribas, A.Cunningham, C. G.Rytuba, J. J.Rye, R. O.Kelly, W. C.Podwysocki, M. H.Mckee, E. H. & Tosdal, R. M. (1995). Geology, geochronology, fluid inclusions, and isotope geochemistry of the Rodalquilar gold alunite deposit, Spain. *Economic Geology,* **90,** 795-822.

Arribas, A.Espinosa, J. & Moro, M. C. (1983). Distribucion de elementos en trazas en las esfaleritas y galenas de las mineralizaclones espanolas asociadas con rocas volcanicas. *Tecniterrae,* **55,** 12-40.

Augier, R. (2004). Evolution tardi-orogénique des Cordillères bétiques (Espagne): Apports d'une étude intégrée. PhD, Université de Pierre et Marie Curie.

Augier, R.Agard, P.Monie, P.Jolivet, L.Robin, C. & Booth-Rea, G. (2005a). Exhumation, doming and slab retreat in the Betic Cordillera (SE Spain): In situ 40Ar/39 AR ages and P-T-d-t paths for the Nevado-Filabride complex. *Journal of Metamorphic Geology,* **23,** 357-381.

Augier, R.Booth-Rea, G.Agard, P.Martinez-Martinez, J. M.Jolivet, L. & Azanon, J. M. (2005b). Exhumation constraints for the lower Nevado-Filabride Complex (Betic Cordillera, SE Spain): a Raman thermometry and Tweequ multiequilibrium thermobarometry approach. *Bulletin de la Societe Geologique de France,* **176,** 403-416.

Augier, R.Jolivet, L. & Robin, C. (2005c). Late Orogenic doming in the eastern Betic Cordilleras: Final exhumation of the Nevado-Filabride complex and its relation to basin genesis. *Tectonics,* **24,** 1-19.

Bakker, H. E.Jong, K. D.Helmers, H. & Biermann, C. (1989). The geodynamic evolution of the Internal Zone of the Betic Cordilleras (south-east Spain): a model based on structural analysis and geothermobarometry. *Journal of Metamorphic Geology,* **7,** 359-381.

Bakker, R. J. (1997). Clathrates: Computer programs to calculate fluid inclusion V-X properties using clathrate melting temperatures. *Computers and Geosciences,* **23,** 1-18.

Bakker, R. J. (1999). Adaptation of the Bowers and Helgeson (1983) equation of state to the H2O-CO2-CH4-N2-NaCl system. *Chemical Geology,* **154,** 225-236.

Bakker, R. J. (2003). Package FLUIDS 1. Computer programs for analysis of fluid inclusion data and for modelling bulk fluid properties. *Chemical Geology,* **194,** 3-23.

Bakker, R. J. & Jansen, J. B. H. (1990). Preferential water leakage from fluid inclusions by means of mobile dislocations. *Nature,* **345,** 58-60.

Bakker, R. J. & Jansen, J. B. H. (1994). A mechanism for preferential H2O leakage from fluid inclusions in quartz, based on TEM observations. *Contributions to Mineralogy and Petrology,* **116,** 7-20.

Banks, D. A.Da Vies, G. R.Yardley, B. W. D.Mccaig, A. M. & Grant, N. T. (1991). The chemistry of brines from an Alpine thrust system in the Central Pyrenees: An application of fluid inclusion analysis to the study of fluid behaviour in orogenesis. *Geochimica et Cosmochimica Acta,* **55,** 1021-1030.

Banks, D. A.Giuliani, G.Yardley, B. W. D. & Cheilletz, A. (2000). Emerald mineralisation in Colombia: fluid chemistry and the role of brine mixing. *Mineralium Deposita,* **35,** 699-713.

Beaudoin, G. (1994). Evidence for an upper crustal source for gold in the Ag-Pb-Zn-Au veins of the Kokanee Range, British Columbia. *Economic Geology,* **89,** 397-400.

Bellon, H.Bordet, P. & Montenat, C. (1983). Chronologie du magmatisme néogène des Cordillères bétiques (Espagne méridionale). *Bulletin de la Societe Geologique de France,* **25,** 205-217.

Benito, R.Lopez-Ruiz, J.Cebria, J. M.Hertogen, J.Doblas, M.Oyarzun, R. & Demaiffe, D. (1999). Sr and O isotope constraints on source and crustal contamination in the high-K calc-alkaline and shoshonitic neogene volcanic rocks of SE Spain. *Lithos,* **46,** 773-802.

Beyssac, O.Bollinger, L.Avouac, J.-P. & Goffé, B. (2004). Thermal metamorphism in the lesser Himalaya of Nepal determined from Raman spectroscopy of carbonaceous material. *Earth and Planetary Science Letters,* **225,** 233-241.

Beyssac, O.Goffé, B.Chopin, C. & Rouzaud, J. N. (2002). Raman spectra of carbonaceous material in metasediments: A new geothermometer. *Journal of Metamorphic Geology,* **20,** 859-871.

Beyssac, O. & Lazzeri, M. (2012). Application of Raman spectroscopy to the study of graphitic carbons in the Earth Sciences. *EMU Notes in Mineralogy,* **12,** 415-454.

Bezada, M.-J.Humphreys, E.-D.Toomey, D.-R.Harnafi, M.Dávila, J.-M. & Gallart, J. (2013). Evidence for slab rollback in westernmost mediterranean from improved upper mantle imaging. *Earth and Planetary Science Letters,* **368,** 51-60.

Bodnar, R. J. (2003). Introduction to aqueous-electrolyte fluid inclusions. *In:* Iain Samson, A. A. A. D. M. (ed.) *Fluid Inclusions : Analysis and Interpretation.* Robert Raeside ed. Vancouver, British Columbia: Mineralogical Association of Canada.

Böhlke, J. K. & Irwin, J. J. (1992). Laser microprobe analyses of noble gas isotopes and halogens in fluid inclusions: Analyses of microstandards and synthetic inclusions in quartz. *Geochimica et Cosmochimica Acta,* **56,** 187-201.

Boiron, M.-C.Cathelineau, M.Banks, D. A.Fourcade, S. & Vallance, J. (2003). Mixing of metamorphic and surficial fluids during the uplift of the Hercynian upper crust: consequences for gold deposition. *Chemical Geology,* **194,** 119-141.

Bolze, J.Ott D'estevou, P.Bordet, P.Montenat, C. & De Larouzière, F. (1986). Processus thermo-mécaniques associés à l'évolution des bassins néogènes des Bétiques internes orientales (Espagne Sud-Est). **Rapport interne n°35,** 92p.

Booth-Rea, G.Azañón, J.-M.Azor, A. & García-Dueñas, V. (2004). Influence of strike-slip fault segmentation on drainage evolution and topography. A case study: the Palomares Fault Zone (southeastern Betics, Spain). *Journal of Structural Geology,* **26,** 1615-1632.

Booth-Rea, G.Azañón, J. M.García-Dueñas, V. & Augier, R. (2003). Uppermost Tortonian to Quaternary depocentre migration related with segmentation of the strike-slip Palomares Fault Zone, Vera Basin (SE Spain). *Comptes Rendus Geosciences,* **335,** 751-761.

Bottrell, S. H.Yardley, B. W. D. & Buckley, F. (1988). A modified crush-leach method for the analysis of fluid inclusion electrolytes. *Bull. Minéral.,* **111,** 279-290.

Boullier, A.-M. (1999). Fluid inclusions: tectonic indicators. *Journal of Structural Geology,* **21,** 1229-1235.

Bourillot, R.Vennin, E.Rouchy, J.-M.Durlet, C.Rommevaux, V.Kolodka, C. & Knap, F. (2009). Structure and evolution of a Messinian mixed carbonate-siliciclastic platform: the role of evaporites (Sorbas Basin, South-east Spain). *Sedimentology,* **57,** 477-512.

Bowers, T. S. & Helgeson, H. C. (1983). Calculation of the thermodynamic and geochemical consequences of nonideal mixing in the system H2O-CO2-NaCl on phase relations in geologic systems: Equation of state for H2O-CO2-NaCl fluids at high pressures and temperatures. *Geochimica et Cosmochimica Acta,* **47,** 1247-1275.

Carrillo-Rosúa, F.-J.Morales-Ruano, S.Esteban-Arispe, I. & Hach-Ali, P. F. (2009). Significance of phyllosilicate mineralogy and mineral chemistry in an epithermal environment. Insights from the Palai-Islica Au-Cu deposit (AlmerÃa, SE Spain). *Clays and Clay Minerals,* **57,** 1-24.

Carrillo-Rosúa, F.-J.Morales-Ruano, S.Fenoll Hach-Alí, P.Boyce, A.-J. & Fallick, A.-E. (2003). Génesis de la barita de Las Herrerías y Sierra Almagrera. *Boletín de la Sociedad Española de Mineralogía,* **26-A,** 159-160.

Carrillo-Rosúa, F.-J.Morales Ruano, S. & Fenoll Hach-Ali, P. (2002). The three generations of gold in the Palai-Islica epithermal deposit, southeastern Spain. *Canadian Mineralogist,* **40,** 1465-1481.

Cathelineau, M.Boiron, M. C.Essarraj, S.Dubessy, J.Lespinasse, M. & Poty, B. (1993). Fluid pressure variations in relation to multistage deformation and uplift; a fluid inclusion study of Au quartz veins. *European Journal of Mineralogy,* **5,** 107-121.

Cesare, B.Rubatto, D. & Gómez-Pugnaire, M. (2009). Do extrusion ages reflect magma generation processes at depth? An example from the Neogene Volcanic Province of SE Spain. *Contributions to Mineralogy and Petrology,* **157,** 267-279.

Clauzon, G. (1980). Révision de l'interprétation géodynamique du passage Miocène - Pliocène dans le bassin de Vera (Espagne méridionale) : les coupes d'Antas et de Cuevas del Almanzora. *Rivista Italiana di Paleontologia,* **86,** 203-214.

Clauzon, G.Suc, J.-P.Gautier, F.Berger, A. & Loutre, M.-F. (1996). Alternate interpretation of the Messinian salinity crisis: Controversy resolved? *Geology,* **24,** 363-366.

Claypool, G. E.Holser, W. T.Kaplan, I. R.Sakai, H. & Zak, I. (1980). The age curves of sulfur and oxygen isotopes in marine sulfate and their mutual interpretation. *Chemical Geology,* **28,** 199-260.

Clayton, R. N. & Mayeda, T. K. (1963). The use of bromine pentafluoride in the extraction of oxygen from oxides and silicates for isotopic analysis. *Geochimica et Cosmochimica Acta,* **27,** 43-52.

Conticelli, S.Guarnieri, L.Farinelli, A.Mattei, M.Avanzinelli, R.Bianchini, G.Boari, E.Tommasini, S.Tiepolo, M.Prelevic, D. & Venturelli, G. (2009). Trace elements and Sr-Nd-Pb isotopes of K-rich, shoshonitic, and calc-alkaline magmatism of the Western Mediterranean Region: Genesis of ultrapotassic to calc-alkaline magmatic associations in a post-collisional geodynamic setting. *Lithos,* **107,** 68-92.

Crespo-Blanc, A.Orozco, M. & Garcia-Dueñas, V. (1994). Extension versus compression during the Miocene tectonic evolution of the Betic chain. Late folding of normal fault systems. *Tectonics,* **13,** 78-88.

De Jong, K. (1991). Tectono-metamorphic studies and radiometric dating in the Betic Cordilleras (SE Spain). Vrije Universiteit.

De Jong, K. (2003). Very fast exhumation of high-pressure metamorphic rocks with excess 40Ar and inherited 87Sr, Betic Cordilleras, southern Spain. *Lithos,* **70,** 91-110.

Demoustier, A.Castroviejo, R. & Charlet, J.-M. (1998). Clasificación textural del cuarzo epitermal (Au-Ag) de relleno filoniano del área volcánica de Cabo de Gata, Almería. *Boletín Geológioco y Minero,* **109,** 449-468.

Diamond, L.Tarantola, A. & Stünitz, H. (2010). Modification of fluid inclusions in quartz by deviatoric stress. II: experimentally induced changes in inclusion volume and composition. *Contributions to Mineralogy and Petrology*.

Dubessy, J. (1984). Simulation des équilibres chimiques dans le système C-O-H. Conséquences méthodologiques pour les inclusions fluides. *Bull. Minéral.,* **107,** 155-168.

Dublyansky, Y. V. & Spötl, C. (2009). Hydrogen and oxygen isotopes of water from inclusions in minerals: design of a new crushing system and on-line continuous-flow isotope ratio mass spectrometric analysis. *Rapid Commun Mass Spectrom,* **23**.

Duggen, S.Hoernle, K.Van Den Bogaard, P. & Garbe-Schonberg, D. (2005). Post-Collisional Transition from Subduction- to Intraplate-type Magmatism in the Westernmost Mediterranean: Evidence for Continental-Edge Delamination of Subcontinental Lithosphere. *Journal of Petrology,* **46,** 1155-1201.

Duggen, S.Hoernle, K.Van Den Bogaard, P. & Harris, C. (2004). Magmatic evolution of the Alboran region: The role of subduction in forming the western Mediterranean and causing the Messinian Salinity Crisis. *Earth and Planetary Science Letters,* **218,** 91-108.

Egeler, C. G. & Simon, O. J. (1969). «Sur la tectonique de la Zone Bétique (Cordillières Bétiques, Espagne). Etudes basées sur la recherche dans le secteur compris entre Almería y Vélez-Rubio». *Verk. Kon. Ned. Akad. V. Wetensch Afd. Nat. serts. reeks.,* **25,** 90 p.

Essarraj, S.Boiron, M.-C.Cathelineau, M.Banks, D. A. & Benharref, M. (2005). Penetration of surface-evaporated brines into the Proterozoic basement and deposition of Co and Ag at Bou

Azzer (Morocco): Evidence from fluid inclusions. *Journal of African Earth Sciences,* **41,** 25-39.

Esteban-Arispe, I.Carrillo-Rosúa, J.Morales-Ruano, S.Velasco-Roldán, F. & Boyce, A.-J. Mineralogy and fluid evolution of Pb-Zn-Cu(Ag-Au) epithermal veins in San José (Almería, Southeastern Spain). Proceedings of the XX European Current Research on Fluid Inclusions, 2009. Fluid and Melt Inclusions: using bubbles to decode the Earth., 79 - 80.

Famin, V.Hébert, R.Philippot, P. & Jolivet, L. (2005). Ion probe and fluid inclusion evidence for co-seismic fluid infiltration in a crustal detachment. *Contributions to Mineralogy and Petrology,* **150,** 354-367.

Famin, V. & Nakashima, S. (2004). Fluid migration in fault zones and the evolution of detachments: The example of Tinos Island (Greece). *In:* Universal Academy Press, I. (ed.) *Physicochemistry of Water in Geological and Biological Systems.* Tokyo, Japan.

Field, C. W. & Fifarek, R. H. (1985). Light stable isotope systematics in the epithermal environment *In:* Berger, B. R., and Bethke, P.M. (ed.) *Geology and Geochemistry of Epithermal Systems, Reviews in Economic Geology.*

Fontes, J. C. & Matray, J. M. (1993). Geochemistry and origin of formation brines from the Paris Basin, France: 1. Brines associated with Triassic salts. *Chemical Geology,* **109,** 149-175.

Fortuin, A. R.Kelling, J. M. D. & Roep, T. B. (1995). The enigmatic Messinian-Pliocene section of Cuevas del Almanzora (Vera Basin, SE Spain) revisited-erosional features and strontium isotope ages. *Sedimentary Geology,* **97,** 177-201.

Garcés, M.Krijgsman, W. & Agusti, J. (1998). Chronology of the late Turolian deposits of the Fortuna basin (SE Spain): implications for the Messinian evolution of the eastern Betics. *Earth and Planetary Science Letters,* **163,** 69-81.

Gargani, J.Moretti, I. & Letouzey, J. (2008). Evaporite accumulation during the Messinian Salinity Crisis: The Suez Rift case. *Geophysical Research Letters,* **35,** L02401.

Gautier, F.Clauzon, G.Suc, J. P.Cravatte, J. & Violanti, D. (1994). Age and duration of the Messinian salinity crisis. *Comptes Rendus de l'Académie des Sciences, Series IIA, Earth and Planetary Science,* **318,** 1103-1109.

Giesemann, A.Jaeger, H. J.Norman, A. L.Krouse, H. R. & Brand, W. A. (1994). Online Sulfur-Isotope Determination Using an Elemental Analyzer Coupled to a Mass Spectrometer. *Analytical Chemistry,* **66,** 2816-2819.

Gomez-Pugnaire, M. T. & Fernandez-Soler, J. M. (1987). High-pressure metamorphism in metabasites from the Betic Cordilleras (S.E. Spain) and its evolution during the Alpine orogeny. *Contributions to Mineralogy and Petrology,* **95,** 231-244.

Gomez-Pugnaire, M. T.Galindo-Zaldivar, J.Rubatto, D.Gonzalez-Lodeiro, F.Lopez Sanchez-Vizcaino, V. & Jabaloy, A. (2004). A reinterpretation of the Nevado-Filabride and Alpujarride Complexes (Betic Cordillera): Field, petrography and U-Pb ages from orthogneisses (western Sierra Nevada, S Spain). *Schweizerische Mineralogische und Petrographische Mitteilungen,* **84,** 303-322.

Gomez-Pugnaire, M. T.Rubatto, D.Fernandez-Soler, J. M.Jabaloy, A.Lopez-Sanchez-Vizcaino, V.Gonzalez-Lodeiro, F.Galindo-Zaldivar, J. & Padron-Navarta, J. A. (2012). Late Variscan magmatism in the Nevado-Filabride Complex: U-Pb geochronologic evidence for the pre-Mesozoic nature of the deepest Betic complex (SE Spain). *Lithos,* **146-147,** 93-111.

Graeser, S. & Friedrich, G. (1970). Zur Frage der Alterstellung und Genese der Blei-Zink-Vorkommen der Sierra de Cartagena in Spanien. *Mineralium Deposita,* **5,** 365-374.

Griveaud, P.Coppier, G.Montenat, C. & Ott D'estevou, P. (1990). Le Néogène des sierras d'Aguilas. *In:* Montenat, C. (ed.) *Les bassins néogènes du domaine Bétique oriental (Espagne).* Doc.et Trav. IGAL ed. Paris.

Hernandez, J.De Larouziere, F. D.Bolze, J. & Bordet, P. (1987). Le magmatisme neogene betico-rifain et le couloir de decrochement trans-Alboran. *Bulletin de la Societe Geologique de France,* **III,** 257-267.

Hollister, L. (1990). Enrichment of CO2 in fluid inclusions in quartz by removal of H2O during crystal-plastic deformation. *Journal of Structural Geology,* **12,** 895-901.
Huizenga, J. M. (2001). Thermodynamic modelling of C-O-H fluids. *Lithos,* **55,** 101-114.
Huizenga, J. M. (2011). Thermodynamic modelling of a cooling C-O-H fluid-graphite system: implications for hydrothermal graphite precipitation. *Mineralium Deposita,* **46,** 23-33.
Ingebritsen, S. E. & Manning, C. E. (2002). Diffuse fluid flux through orogenic belts: Implications for the world ocean. *Proceedings of the National Academy of Sciences USA,* **99,** 9,113-9,116.
Jabaloy, A.Galindo-Zaldívar, J. & González-Lodeiro, F. (1993). The Alpujárride-Nevado-Fibábride extensional shear zone, Betic Cordillera, SE Spain. *Journal of Structural Geology,* **15,** 555-569.
Jessell, M. W. (1987). Grain-boundary migration microstructures in a naturally deformed quartzite. *Journal of Structural Geology,* **9,** 1007-1014.
Johnson, E. L. & Hollister, L. S. (1995). Syndeformational fluid trapping in quartz: determining the pressure- temperature conditions of deformation from fluid inclusions and the formation of pure CO2 fluid inclusions during grain-boundary migration. *Journal of Metamorphic Geology,* **13,** 239-249.
Jolivet, L.Augier, R.Faccenna, C.Negro, F.Rimmele, G.Agard, P.Robin, C.Rossetti, F. & Crespo-Blanc, A. (2008). Subduction, convergence and the mode of backarc extension in the Mediterranean region. *Bulletin de la Societe Geologique de France,* **179,** 525-550.
Kerrich, R. (1976). Some effects of tectonic recrystallisation on fluid inclusions in vein quartz. *Contributions to Mineralogy and Petrology,* **59,** 195-202.
Krantz, R. L. (1983). Microcracks in rocks: a review. *Tectonophysics,* **100,** 449-480.
Krijgsman, W.Garcés, M.Agusti, J.Raffi, I.Taberner, C. & Zachariasse, W. J. (2000). The "Tortonian salinity crisis" of the eastern Betics (Spain). *Earth and Planetary Science Letters,* **181,** 497-511.
Krijgsman, W.Hilgen, F. J.Raffi, I.Sierro, F. J. & Wilson, D. S. (1999). Chronology, causes and progression of the Messinian salinity crisis. *Nature,* **400,** 652-655.
Leisen, M.Boiron, M.-C.Richard, A. & Dubessy, J. (2012a). Determination of Cl and Br concentrations in individual fluid inclusions by combining microthermometry and LA-ICPMS analysis: Implications for the origin of salinity in crustal fluids. *Chemical Geology,* **330-331,** 197-206.
Leisen, M.Dubessy, J.Boiron, M.-C. & Lach, P. (2012b). Improvement of the determination of element concentrations in quartz-hosted fluid inclusions by LA-ICP-MS and Pitzer thermodynamic modeling of ice melting temperature. *Geochimica et Cosmochimica Acta,* **90,** 110-125.
Lespinasse, M. (1999). Are fluid inclusion planes useful in structural geology? *Journal of Structural Geology,* **21,** 1237-1243.
Lespinasse, M.Désindes, L.Fratczak, P. & Petrov, V. (2005). Microfissural mapping of natural cracks in rocks: Implications for fluid transfers quantification in the crust. *Chemical Geology,* **223,** 170-178.
Lister, G. S. & Davis, G. A. (1989). The origin of metamorphic core complexes and detachment faults formed during Tertiary continental extension in the northern Colorado River region, U.S.A. *Journal of Structural Geology,* **11,** 65-94.
Lonergan, L. & Mange-Rajetzky, M. A. (1994). Evidence for Internal Zone unroofing from foreland basin sediments, Betic Cordillera, SE Spain. *Journal of the Geological Society,* **151,** 515-529.
Lonergan, L. & White, N. (1997). Origin of the Betic-Rif mountain belt. *Tectonics,* **16,** 504-522.
Lopez Ruiz, J. & Rodriguez Badiola, E. (1980). La region volcanica neogena del sureste de Espana. *Estudios Geologicos,* **36,** 5-63.
Manning, C. E. & Ingebritsen, S. E. (1999). Permeability of the continental crust: The implications of geothermal data and metamorphic systems. *Reviews of Geophysics,* **37,** 127-150.

Martínez-Frías, J. (1998). An ancient Ba-Sb-Ag-Fe-Hg-bearing hydrothermal system in SE Spain. *Episodes,* **21,** 248-251.

Martinez-Frias, J.Delgado-Huertas, A.Garcia-Moreno, F.Reyes, E.Lunar, R. & Rull, F. (2007). Isotopic signatures of extinct low-temperature hydrothermal chimneys in the Jaroso Mars analog. *Planetary and Space Science,* **55,** 441-448.

Martínez-Martínez, J. M. & Azañón, J. M. (2002). Orthogonal extension in the hinterland of the Gibraltar Arc (Betics, SE Spain), in Reconstruction of the evolution of the Alpine-Himalayan Orogen. *Journal of the Virtual Explorer,* **8,** 3-22.

Martínez-Martínez, J. M.Soto, J. I. & Balanya, J. C. (2002). Orthogonal folding of extensional detachments: Structure and origin of the Sierra Nevada elongated dome (Betics, SE Spain). *Tectonics,* **21**.

Martinez Frias, J.Garcia Guinea, J.Lopez Ruiz, J.Lopez Garcia, J. Á. & Benito Garcia, R. (1989). Las mineralizaciones epitermales de Sierra Almagrera y de la cuenca de Herrerías, Cordilleras Béticas. *Bol. Soc. Esp. Mineral. ,* **12,** 261-271.

Massonne, H.-J. & Schreyer, W. (1987). Phengite geobarometry based on the limiting assemblage with K-feldspar, phlogopite, and quartz. *Contributions to Mineralogy and Petrology,* **96,** 212-224.

Mccaig, A. M.Tritlla, J. & Banks, D. A. (2000). Fluid mixing and recycling during Pyrenean thrusting: evidence from fluid inclusion halogen ratios. *Geochimica et Cosmochimica Acta,* **64,** 3395-3412.

Menzies, C. D.Teagle, D. A. H.Craw, D.Cox, S. C.Boyce, A. J.Barrie, C. D. & Roberts, S. (2014). Incursion of meteoric waters into the ductile regime in an active orogen. *Earth and Planetary Science Letters,* **399,** 1-13.

Montenat, C. & Ott D'estevou, P. (1990). Eastern Betic Neogene basins-a review. *D.E.T.I.s (Ed.) : Les bassins néogènes de domaines bétique oriental (Espagne),* **12-13,** 9-15.

Montenat, C.Ott D'estevou, P.De Larouzière, F. & Bedu, P. (1987). Originalité géodynamique des bassins néogènes de domaine oriental (Espagne). *Extrait de "Notes et Mémoires",* **21**.

Morales Ruano, S. (1994). Mineralogia, geocuimica y metalogenia de los yacimientos hidrothermales del sureste de Espana (Aguilas-Sierra Almagrera. Universidad de Granada.

Morales Ruano, S.Both, R. & Fenoll Hach-Ali, P. (1993). Paragenesis and regional zoning of the polymetallic ore deposits in the Aguilas and Sierra Almagrera-Herrerias areas, Southeastern Spain. 171-174.

Morales Ruano, S.Both, R. & Fenoll Hach-Ali, P. (1995). Fluid evolution and mineral deposition in the Aguilas – Sierra Almagrera base metal ores, southeastern Spain. *Mineral Deposits***,** 365-368.

Morales Ruano, S.Rosua, F. J. C.Hach-Ali, P. F.Chacon, F. D. L. F. & Lopez, E. C. (2000). Epithermal Cu-Au mineralization in the Palai-Islica deposit, Almeria, southeastern Spain: Fluid-inclusion evidence for mixing of fluids as a guide to gold mineralization. *Canadian Mineralogist,* **38,** 553-565.

Morrison, J. & Anderson, J. L. (1998). Footwall refrigeration along a detachment fault: implications for thermal evolution of core complexes. *Science,* **279,** 63-66.

Mulch, A.Teyssier, C.Cosca, M.Vanderhaeghe, O. & Vennemann, T. (2004). Reconstructing paleoelevation in eroded orogens. *Geology,* **32,** 525-528.

Oen, I. S.Fernandez, J. C. & Manteca, J. I. (1975). The lead-zinc and associated ores of La Union-Sierra de Cartagena, Spain. *Economic Geology,* **70,** 1259-1278.

Omodeo Salé, S.Gennari, R.Lugli, S.Manzi, V. & Roveri, M. (2012). Tectonic and climatic control on the Late Messinian sedimentary evolution of the Nijar Basin (Betic Cordillera, Southern Spain). *Basin Research,* **24,** 314-337.

Passchier, C. W. & Trouw, R. A. J. (2005). Microtectonics.

Pedrera, A.Galindo-Zaldivar, J.Tello, A. & Marin-Lechado, C. (2010). Intramontane basin development related to contractional and extensional structure interaction at the termination

of a major sinistral fault: The Huercal-Overa Basin (Eastern Betic Cordillera). *Journal of Geodynamics,* **49,** 271-286.

Platt, J. P. (2007). From orogenic hinterlands to Mediterranean-style back-arc basins: a comparative analysis. *Journal of the Geological Society,* **164,** 297-311.

Platt, J. P.Anczkiewicz, R.Soto, J. I.Kelley, S. P. & Thirlwall, M. (2006). Early Miocene continental subduction and rapid exhumation in the western Mediterranean. *Geology,* **34,** 981-984.

Platt, J. P. & Vissers, R. L. M. (1989). Extensional collapse of thickened continental lithosphere: A working hypothesis for the Alboran Sea and Gibraltar arc. *Geology,* **17,** 540-543.

Prelevic, D.Foley, S. F.Romer, R. & Conticelli, S. (2008). Mediterranean Tertiary lamproites derived from multiple source components in postcollisional geodynamics. *Geochimica et Cosmochimica Acta,* **72,** 2125-2156.

Rouchy, J. M.Taberner, C.Blanc-Valleron, M.-M.Sprovieri, R.Russell, M.Pierre, C.Di Stefano, E.Pueyo, J. J.Caruso, A.Dinarã¨S-Turell, J.Gomis-Coll, E.Wolff, G. A.Cespuglio, G.Ditchfield, P.Pestrea, S.Combourieu-Nebout, N.Santisteban, C. & Grimalt, J. O. (1998). Sedimentary and diagenetic markers of the restriction in a marine basin: The Lorca Basin (SE Spain) during the Messinian. *Sedimentary Geology,* **121,** 23-55.

Scheppard, S. & Schwarcz, H. (1970). Fractionation of carbon and oxygen isotopes and magnesium between coexistang metamorphic calcite and dolomite. *Contributions to Mineralogy and Petrology,* **26,** 161-198.

Seidenkrantz, M. S.Kouwenhoven, T. J.Jorissen, F. J.Shackleton, N. J. & Van Der Zwaan, G. J. (2000). Benthic foraminifera as indicators of changing Mediterranean-Atlantic water exchange in the late Miocene. *Marine Geology,* **163,** 387-407.

Sheppard, S. (1986). Characterization and isotopic variations in natural waters. *In:* Mineral., M. S. A. R. (ed.) *Stable Isotopes in High Temperature Geological Processes.* Washington,D.C.

Siebenaller, L.Boiron, M. C.Vanderhaeghe, O.Hibsch, C.Jessell, M. W.Andre-Mayer, A. S.France-Lanord, C. & Photiades, A. (2013). Fluid record of rock exhumation across the brittle–ductile transition during formation of a Metamorphic Core Complex (Naxos Island, Cyclades, Greece). *Journal of Metamorphic Geology,* **31,** 313-338.

Stipp, M. & Kunze, K. (2008). Dynamic recrystallization near the brittle-plastic transition in naturally and experimentally deformed quartz aggregates. *Tectonophysics,* **448,** 77-97.

Tarantola, A.Diamond, L. & Stünitz, H. (2010). Modification of fluid inclusions in quartz by deviatoric stress I: experimentally induced changes in inclusion shapes and microstructures. *Contributions to Mineralogy and Petrology*.

Tarantola, A.Diamond, L. W.Stünitz, H.A., T. & Pec, M. (2012). Modification of fluid inclusions in quartz by deviatoric stress III: Influence of principal stresses on inclusion density and orientation. *Contributions to Mineralogy and Petrology*.

Tarantola, A.Mullis, J.Vennemann, T.Dubessy, J. & De Capitani, C. (2007). Oxidation of methane at the CH4/H2O-(CO2) transition zone in the external part of the Central Alps, Switzerland: Evidence from stable isotope investigations. *Chemical Geology,* **237,** 329-357.

Turner, S. P.Platt, J. P.George, R. M. M.Kelley, S. P.Pearson, D. G. & Nowell, G. M. (1999). Magmatism Associated with Orogenic Collapse of the Betic Alboran Domain, SE Spain. *Journal of Petrology,* **40,** 1011-1036.

Ulrich, M. R. & Bodnar, R. J. (1988). Systematics of stretching of fluid inclusions. II. Barite at one atmosphere confining pressure. *Economic Geology,* **83,** 1037-1046.

Van Den Kerkhof, A. M. & Hein, U. F. (2001). Fluid inclusion petrography. *Lithos,* **55,** 27-47.

Vanderhaeghe, O. & Teyssier, C. (2001). Crustal-scale rheological transitions during late-orogenic collapse. *Tectonophysics,* **335,** 211-228.

Vityk, M.Bodnar, R. J. & Dudok, I. (1995). Natural and synthetic re-equilibration textures of fluid inclusions in quartz (Marmarosh Diamonds): Evidence for refillingunder conditions of compressive loading. *European Journal of Mineralogy,* **7,** 1071-1087.

Weijermars, R. (1985). Uplift history of a Betic fold nappe inferred from Neogene- Quaternary sedimentation and tectonics (in the Sierra Alhamilla and Almeria, Sorbas and Tabernas basins of the Betic Cordilleras, SE Spain. *Geologie en Mijnbouw,* **64,** 397-411.

Wernicke, B. & Burchfiel, B. C. (1982). Modes of extensional tectonics. *Journal of Structural Geology,* **4,** 105-115.

Westra, G. (1969). Petrogenesis of a composite metamorphic facies series in an intricate fault zone of the southeastern Sierra Cabrera (SE, Spain). PhD, Amsterdam.

Wilkins, R. W. T. & Barkas, J. P. (1978). Fluid inclusions, deformation and recrystallization in granite tectonites. *Contributions to Mineralogy and Petrology,* **65,** 293-299.

Yardley, B. W. D. (2005). 100th Anniversary Special Paper: Metal Concentrations in Crustal Fluids and Their Relationship to Ore Formation. *Economic Geology,* **100,** 613-632.

Zeck, H. P.Maluski, H. & Kristensen, A. B. (2000). Revised geochronology of the Neogene calc-alkaline volcanic suite in Sierra de Gata, Alborán volcanic province, SE Spain. *Journal of the Geological Society, London,* **157,** 75-81.

Zhang, Y.-G. & Frantz, J. D. (1987). Determination of the homogenization temperatures and densities of supercritical fluids in the system NaClKClCaCl2H2O using synthetic fluid inclusions. *Chemical Geology,* **64,** 335-350.

Zheng, Y.-F. (1993). Calculation of oxygen isotope fractionation in anhydrous silicate minerals. *Geochimica et Cosmochimica Acta,* **57,** 1079-1091.

Figure 1:a) Geological context of the Eastern Betics and location of the Sierra Almagrera (modified after Augier (2004)). b) Geological map of the Sierra Almagrera, Vera basin and Palomares fault zone (modified after Booth-Rea (2004) and Montenat & Ott D'estevou (1990), and location of sampling areas. c) Poles of mineralized V-ore veins (barite and siderite) in El Arteal tunnel represented on lower-hemisphere stereogram.

Figure 2: a) V-Qtz1 quartz vein parallel to the rock foliation. b) Optical microphotograph under cross-polarized light (XPL) showing petrography of Qtz1: static recrystallization (120° angles) and grain boundary migration recrystallization. c) Qtz1: recrystallised quartz with transgranular FIP. d) Qtz1-tg1 FIP. e) Qtz1-tg2 FIP. f) Pole projections of Qtz1-tg1 and Qtz1-tg2 fluid inclusion planes represented on lower hemisphere stereogram. Arrows indicate the directions of opening. L for liquid, V for vapour and S for solid.

Figure 3: a) V-Qtz2 quartz vein locally parallel to the foliation (upper part), while the main section is discordant to the foliation (central part). b) Relationship between petrography of recrystallised quartz (subgrain rotation and bulging) and fluid inclusions. c) Optical microphotographs under plane-polarized light showing intragranular Qtz2-ig. d) Deformed fluid inclusion Qtz2-ig. e) Pole projections of Qtz2-ig fluid inclusion planes represented on lower-hemisphere stereogram.

Figure 4: a) N10E V-Qtz2 discordant to the foliation reopened as V-Qtz3, intersected by V-ore discordant vein. Optical microphotographs under natural light: b) Contact between Qtz2 and Qtz3. Qtz2 grains still showing undulose extinction and affected by Qtz2-tg. Qtz3 euhedral quartz containing only Qtz3-p primary fluid inclusions. Hematite microfissures affecting Qtz2. Hematite also filling open spaces between Qtz3 crystals. c) Zoom of zone localized in b). d) Hematite in reflected light. e) Qtz2-tg. f) Qtz3-p.

Figure 5: Optical microphotographs of V-ore and related minerals, in plane-polarized light (PPL), cross-polarized light (XPL) and reflected light (RL). a) Vein of siderite and micro-euhedral quartz (XPL). b) Sequence of siderite, galena and barite (PPL+ RL). c) Schematic representation of chloritoid-schist breccia cemented by various minerals (V-ore). d) Sd-p primary fluid inclusion in siderite. e) Brt-p in barite.

Figure 6: a) V-Qtz2 oblique quartz vein intersected by V-Cal oblique calcite vein. b) Relationships between V-Qtz2 grains, Qtz2-tg and calcite vein containing Cal-p. c) Detail of Cal-p.

Figure 7: Microthermometry and salinity data for all types of fluid inclusions from the Sierra Almagrera.

Figure 8: Cl/Br molar ratio vs. Cl concentration for fluid inclusions analysed both by LA-ICP-MS (empty symbols) and crush-leach methods (CL, full symbols) (samples from the mining district). The seawater evaporation trend is indicated (Fontes & Matray, 1993) as SW: Seawater, G: Gypsum, H: Halite, E: Epsomite, S: Sylvite, C: Carnallite, B: Bischofite. Comparison data (crush-leach analysis) in boxes 1 to 4: 1—Variscan fluids equilibrated with host rocks (granite and metamorphic rocks), (Boiron *et al.*, 2003), 2—Primary brines derived from Triassic evaporites in the Pyrenees (Mccaig *et al.*, 2000), 3—Primary brines from Ag deposits in Morocco (Essarraj *et al.*, 2005), 4—Secondary brines associated with emerald mineralization in Columbia (Banks *et al.*, 2000).

Figure 9 : Box-and-whisker plots showing the concentrations of various elements concentrations (in ppm) in fluid inclusions Qtz1-tg1, Qtz2-tg, Qtz3-p and Brt-p obtained by LA-ICP-MS method (other FI did provide significant signal). Sr and Ba concentrations are not significant for Brt-p because of the presence of the element in the ablated mineral matrix. Lower whiskers, bottoms of boxes, red central lines, tops of boxes and upper whiskers represent 10th, 25th, 50th, 75th and 90th percentiles respectively. n, number of fluid inclusions analysed, it is identical for all the elements.

Figure 10: $\delta^{18}O_{fluid}$ ‰ $_{V\text{-}SMOW}$ vs. δD_{fluid} ‰ $_{V\text{-}SMOW}$ for Qtz2-ig, Qtz3-p and Sd-p fluids. Fields of some representative fluids from the literature: basinal fluids (Sheppard (1986): GC = Gulf Coast; C = California; M= Michigan). Metamorphic and magmatic fluids boxes are plotted from Field and Fifarek (1985).

Figure 11: *P* (MPa) vs. *T* (°C) of fluid inclusion stages in the Sierra Almagrera. l.p.: geothermal gradient at lithostatic pressure; h.p.: geothermal gradient at hydrostatic pressure.

Figure 12: Exhumation of the Sierra Almagrera with associated tectonic regime, paleo-orographic evolution and paleofluid sequence

Table 1: Abbreviations referring to microthermometric experiments. .

Table 2: Nomenclature, location and description of sampled veins

Table 3: Nomenclature, chronology and characteristics of fluid inclusions. Abbreviations: -tg stands for transgranular, -ig for intragranular and -p for primary, L: liquid, V: vapour, acc.: accidentally trapped mineral, Sd: siderite, Brt: barite, Cal: calcite.

Table 4: Microthermometric and compositional data for all generations of fluid inclusions from the Sierra Almagrera (values of mode in italics). - : not determined

Table 5: LA-ICP-MS data for four generations of fluid inclusions from the Sierra Almagrera. Concentrations are given in ppm and Na/K are mass ratios. - : not determined

Table 6: Isotopic data for various stages of fluid inclusions from the Sierra Almagrera, - : not determined.

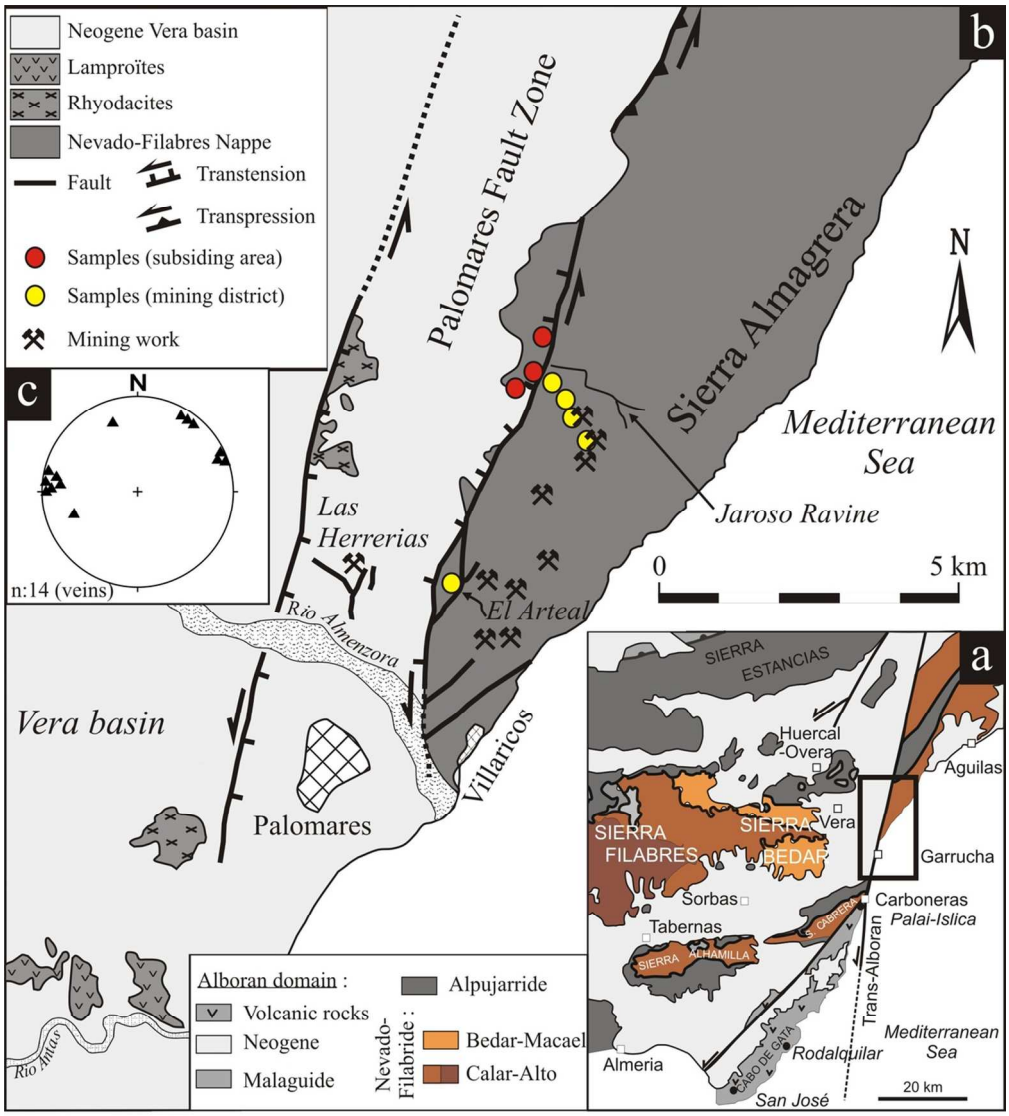

a) Geological context of the Eastern Betics and location of the Sierra Almagrera (modified after Augier (2004)). b) Geological map of the Sierra Almagrera, Vera basin and Palomares fault zone (modified after Booth-Rea (2004) and Montenat & Ott D'estevou (1990), and location of sampling areas. c) Poles of mineralized V-ore veins (barite and siderite) in El Arteal tunnel represented on lower-hemisphere stereogram.
109x121mm (300 x 300 DPI)

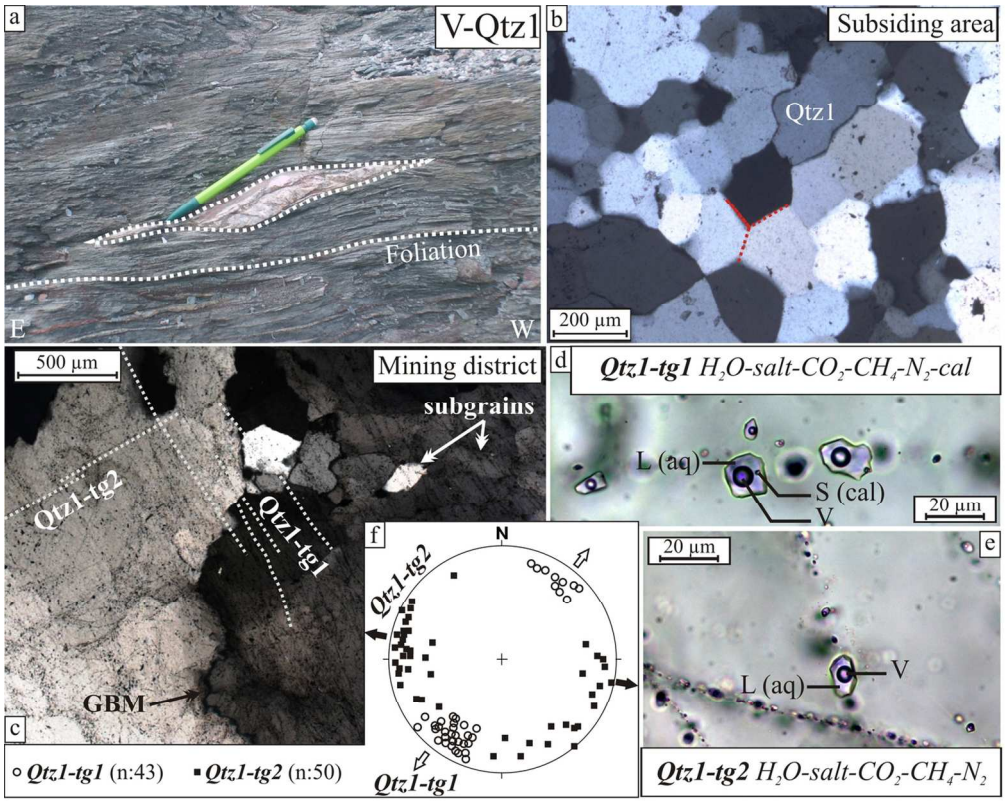

a) V-Qtz1 quartz vein parallel to the rock foliation. b) Optical microphotograph under cross-polarized light (XPL) showing petrography of Qtz1: static recrystallization (120° angles) and grain boundary migration recrystallization. c) Qtz1: recrystallised quartz with transgranular FIP. d) Qtz1-tg1 FIP. e) Qtz1-tg2 FIP. f) Pole projections of Qtz1-tg1 and Qtz1-tg2 fluid inclusion planes represented on lower hemisphere stereogram. Arrows indicate the directions of opening. L for liquid, V for vapour and S for solid.
126x100mm (300 x 300 DPI)

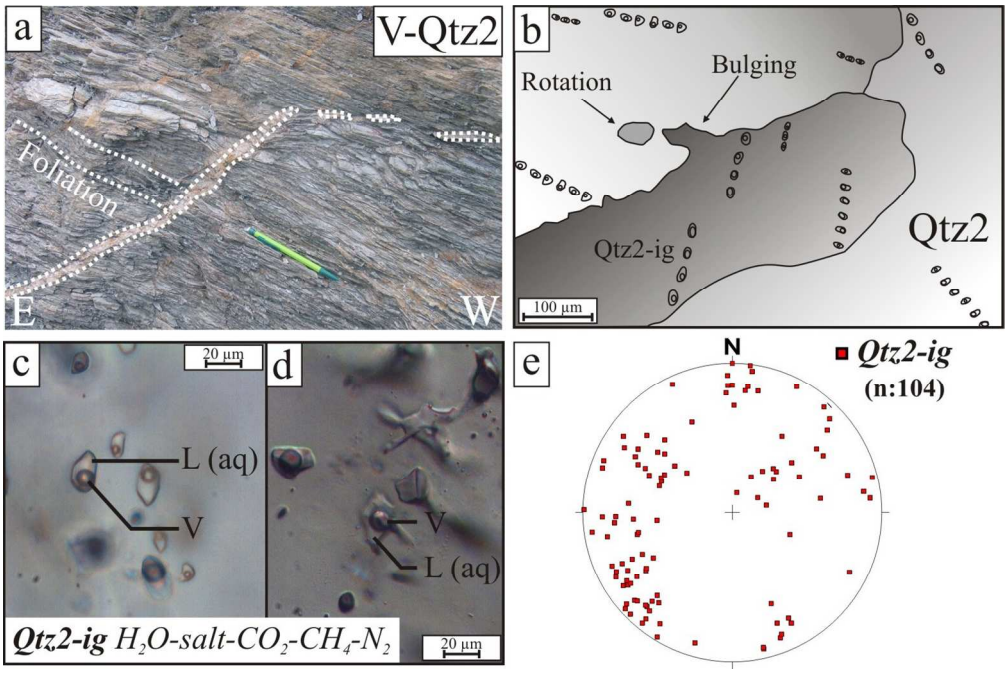

a) V-Qtz2 quartz vein locally parallel to the foliation (upper part), while the main section is discordant to the foliation (central part). b) Relationship between petrography of recrystallised quartz (subgrain rotation and bulging) and fluid inclusions. c) Optical microphotographs under plane-polarized light showing intragranular Qtz2-ig. d) Deformed fluid inclusion Qtz2-ig. e) Pole projections of Qtz2-ig fluid inclusion planes represented on lower-hemisphere stereogram.
133x88mm (300 x 300 DPI)

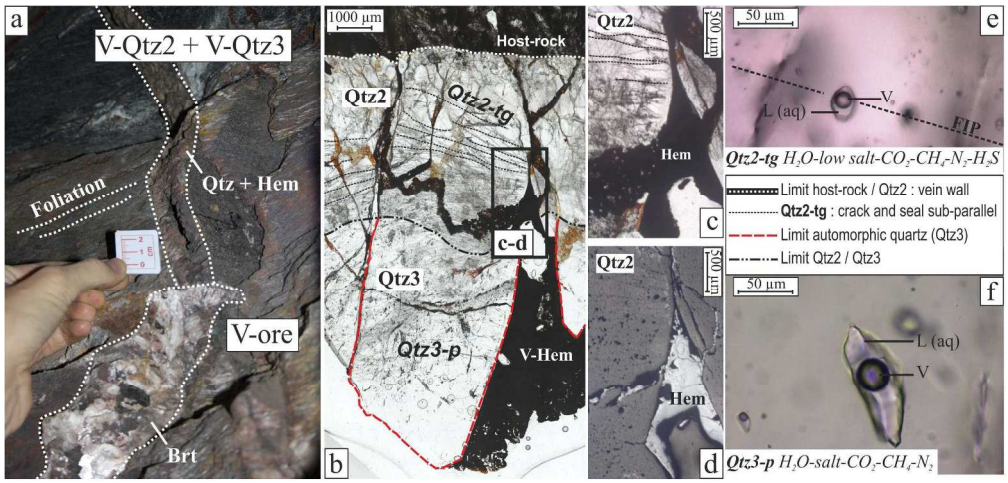

a) N10E V-Qtz2 discordant to the foliation reopened as V-Qtz3, intersected by V-ore discordant vein. Optical microphotographs under natural light: b) Contact between Qtz2 and Qtz3. Qtz2 grains still showing undulose extinction and affected by Qtz2-tg. Qtz3 euhedral quartz containing only Qtz3-p primary fluid inclusions. Hematite microfissures affecting Qtz2. Hematite also filling open spaces between Qtz3 crystals. c) Zoom of zone localized in b). d) Hematite in reflected light. e) Qtz2-tg. f) Qtz3-p.
239x113mm (300 x 300 DPI)

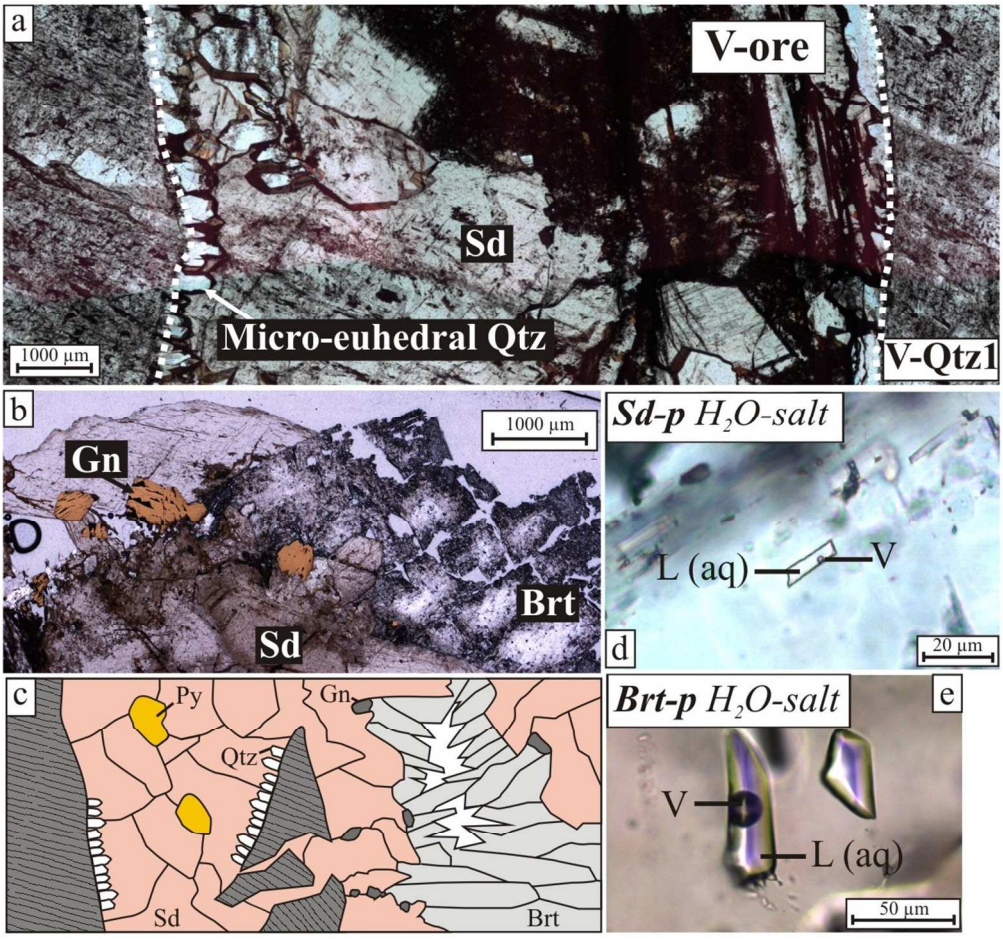

Optical microphotographs of V-ore and related minerals, in plane-polarized light (PPL), cross-polarized light (XPL) and reflected light (RL). a) Vein of siderite and micro-euhedral quartz (XPL). b) Sequence of siderite, galena and barite (PPL+ RL). c) Schematic representation of chloritoid-schist breccia cemented by various minerals (V-ore). d) Sd-p primary fluid inclusion in siderite. e) Brt-p in barite.
110x103mm (300 x 300 DPI)

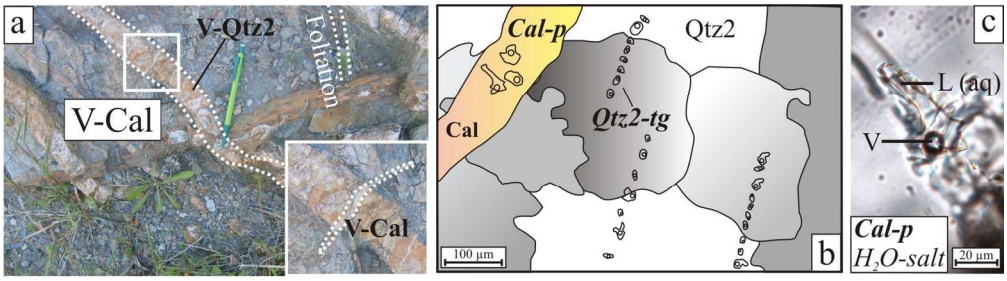

a) V-Qtz2 oblique quartz vein intersected by V-Cal oblique calcite vein. b) Relationships between V-Qtz2 grains, Qtz2-tg and calcite vein containing Cal-p. c) Detail of Cal-p.
161x44mm (300 x 300 DPI)

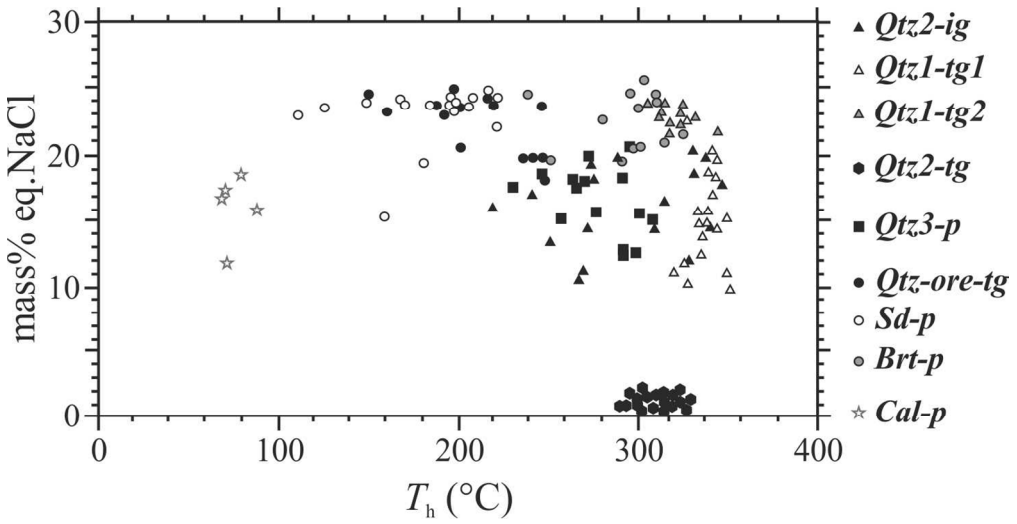

Microthermometry and salinity data for all types of fluid inclusions from the Sierra Almagrera.
124x63mm (300 x 300 DPI)

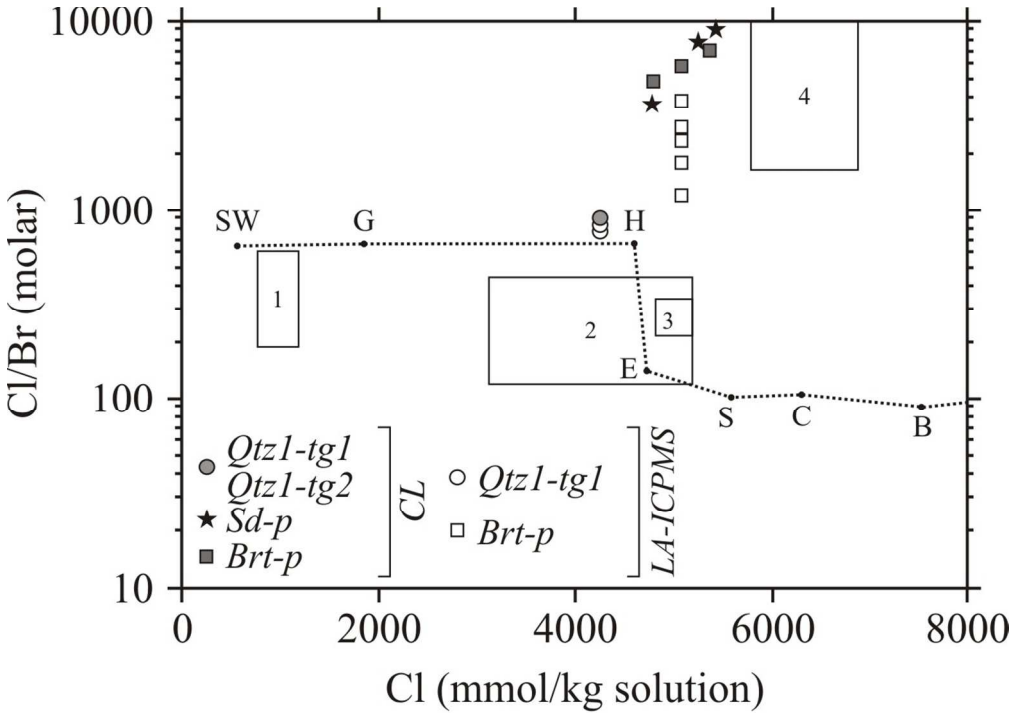

Cl/Br molar ratio vs. Cl concentration for fluid inclusions analysed both by LA-ICP-MS (empty symbols) and crush-leach methods (CL, full symbols) (samples from the mining district). The seawater evaporation trend is indicated (Fontes & Matray, 1993) as SW: Seawater, G: Gypsum, H: Halite, E: Epsomite, S: Sylvite, C: Carnallite, B: Bischofite. Comparison data (crush-leach analysis) in boxes 1 to 4: 1—Variscan fluids equilibrated with host rocks (granite and metamorphic rocks), (Boiron et al., 2003), 2—Primary brines derived from Triassic evaporites in the Pyrenees (Mccaig et al., 2000), 3—Primary brines from Ag deposits in Morocco (Essarraj et al., 2005), 4—Secondary brines associated with emerald mineralization in Columbia (Banks et al., 2000).
116x82mm (300 x 300 DPI)

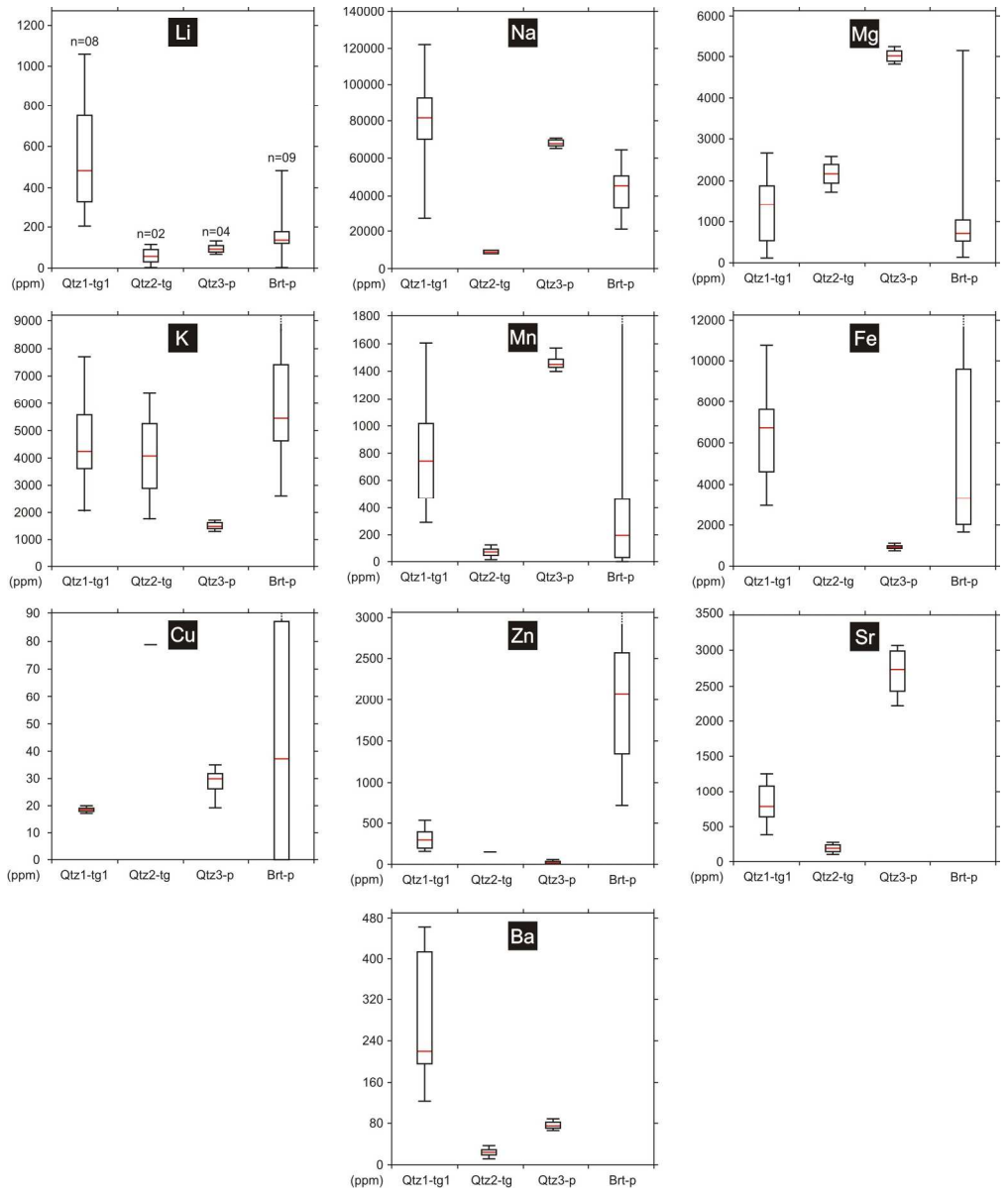

Box-and-whisker plots showing the concentrations of various elements concentrations (in ppm) in fluid inclusions Qtz1-tg1, Qtz2-tg, Qtz3-p and Brt-p obtained by LA-ICP-MS method (other FI did provide significant signal). Sr and Ba concentrations are not significant for Brt-p because of the presence of the element in the ablated mineral matrix. Lower whiskers, bottoms of boxes, red central lines, tops of boxes and upper whiskers represent 10th, 25th, 50th, 75th and 90th percentiles respectively. n, number of fluid inclusions analysed, it is identical for all the elements.
194x231mm (300 x 300 DPI)

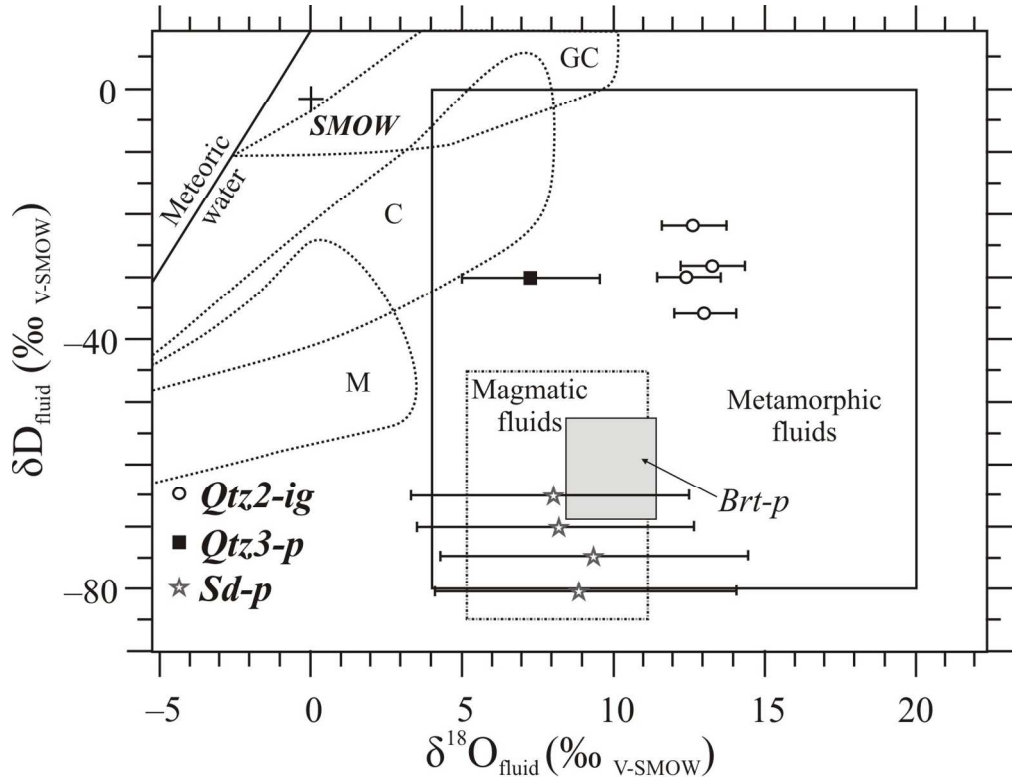

δ18Ofluid ‰ V-SMOW vs. δDfluid ‰ V-SMOW for Qtz2-ig, Qtz3-p and Sd-p fluids. Fields of some representative fluids from the literature: basinal fluids (Sheppard (1986): GC = Gulf Coast; C = California; M= Michigan). Metamorphic and magmatic fluids boxes are plotted from Field and Fifarek (1985).
146x113mm (300 x 300 DPI)

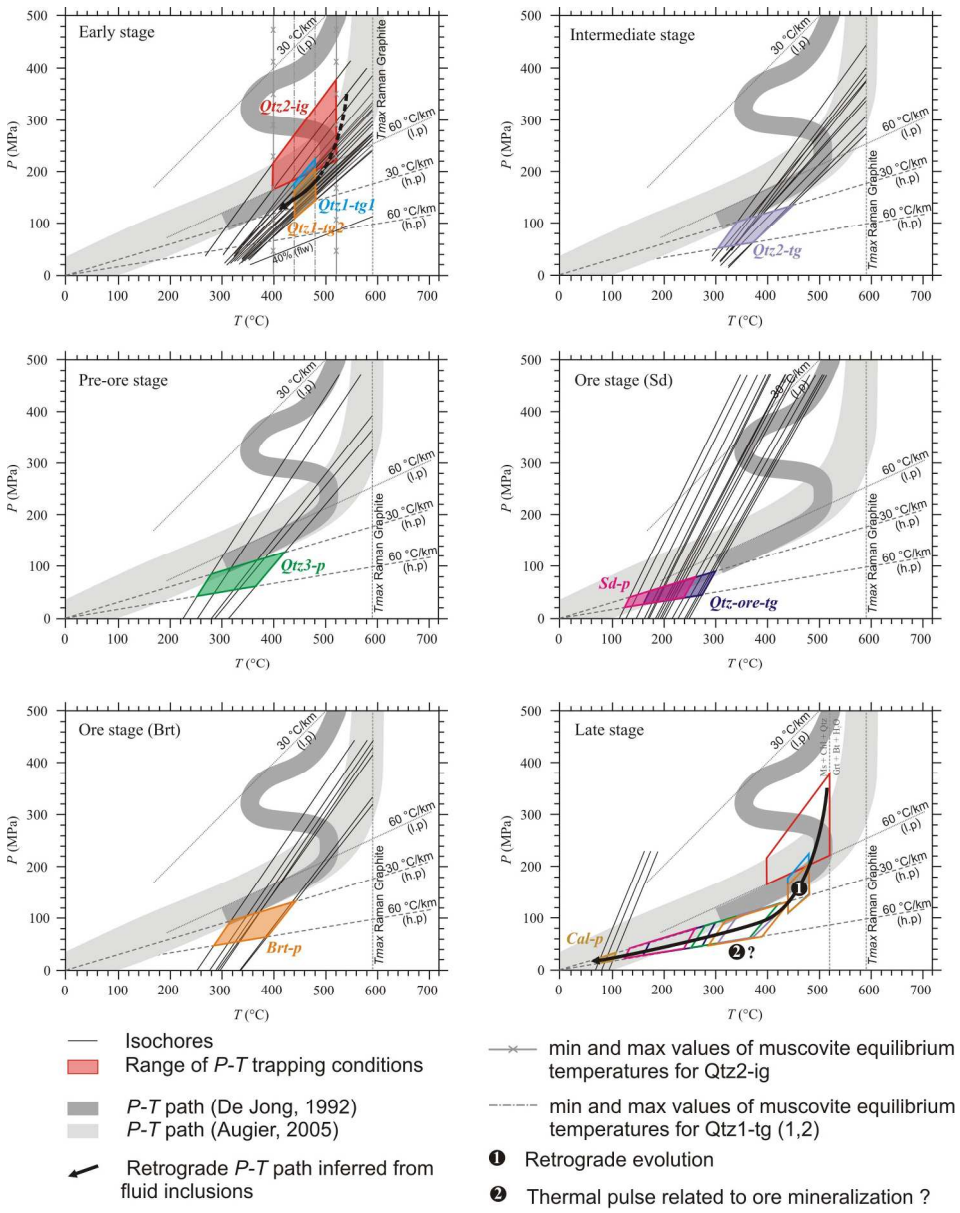

P (MPa) vs. T (°C) of fluid inclusion stages in the Sierra Almagrera. l.p.: geothermal gradient at lithostatic pressure; h.p.: geothermal gradient at hydrostatic pressure.
196x248mm (300 x 300 DPI)

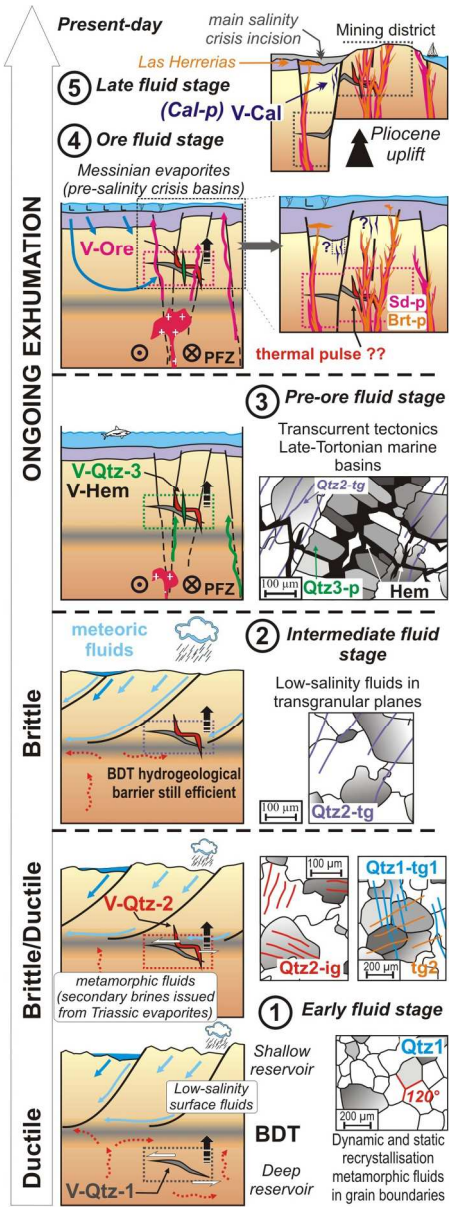

Exhumation of the Sierra Almagrera with associated tectonic regime, paleo-orographic evolution and paleofluid sequence
77x208mm (300 x 300 DPI)

Abbreviation	Observation
-p	Primary fluid inclusion
-ig	Intragranular fluid inclusion plane
-tg	Transgranular fluid inclusion plane
L	Liquid
V	Vapour
S	Solid
flw	Volume fraction of aqueous liquid
T_e	Eutectic or apparent eutectic temperature. First formation of visible liquid of solid aqueous phase on heating
T_m(ice)	Final melting temperature of solid aqueous phase
T_m(cla)	Dissociation temperature of clathrate
T_h(L)	Bulk homogenization temperature via bubble-point transition (L+V=L)
T_h(V)	Bulk homogenization temperature via dew-point transition (L+V=V)

1 Table: Abbreviations referring to microthermometric experiments. .

Vein type and chronology	Location	Vein / rock foliation relationships	Vein mineralogy (this study)
V-Qtz1	Subsident area	Parallel to the rock foliation	Quartz (Qtz1)
	Mining district	Parallel	Quartz (Qtz1)
V-Qtz2	Subsident area	Parallel to oblique	Quartz (Qtz2)
	Mining district	Parallel to oblique	Quartz (Qtz2)
V-Qtz3	Mining district	Oblique	Quartz (Qtz3), Hematite
V-ore	Mining district	Oblique	Quartz, Siderite, Pyrite, Galena, Barite
V-Cal	Subsident area	Oblique	Calcite

1 Table: Nomenclature, location and description of sampled veins

Vein type and chronology	Fluid inclusion petrography	Strike direction	Size (μm)	Shape	Filling	Flw (vol %)
V-Qtz1	-	Grain boundary	?		?	?
	Qtz1-tg1	N130°	~20	Equant, rounded	L, V, acc.	65-75
				Euhedral	calcite	65-75
	Qtz1-tg2	N000° - N030°	15-25		L, V	
V-Qtz2	Qtz2-ig	Random	15-25	Euhedral to dismembered	L, V	50-80
	Qtz2-tg	N000° - N010°	10-15	Equant, rounded	L, V	70-80
V-Qtz3	Qtz3-p	Primary inclusions	>50	Elongated	L, V	70-75
V-ore	Qtz-ore-tg	N000° - N010°	5-10	Euhedral	L, V	70-90
	Sd-p	Primary (cleavage planes)	5-20	Euhedral, flat	L, V	70-90
	Brt-p	Primary (cleavage planes)	30-50	Euhedral, irregular	L or L, V	65-80
V-Cal	Cal-p	Isolated clusters	20-70	Irregular, flat	?	80-95

Table: Nomenclature, chronology and characteristics of fluid inclusions. Abbreviations: -tg stands for transgranular, -ig for intragranular and -p for primary, L: liquid, V: vapour, acc.: accidentally trapped mineral, Sd: siderite, Brt: barite, Cal: calcite.

		Microthermometry					Calculated composition						
Fluid inclusion petrography	Fluid inclusion type	T_e (°C)	T_m(Ice) (°C)	T_m(Cla) (°C)	T_h (°C)	Salinity (mass% eq. NaCl)	V_m (cm^3/mol)	H_2O (mol %)	CO_2 (mol %)	CH_4 (mol %)	N_2 (mol %)	H_2S (mol %)	NaCl (mol %)
Qtz1-tg1	Aqueous carbonic	-48.6/-39.8 *-45.2*	-22.7/-7.7 *-14.5*	-3.8/6.5 *6.0*	319/350 *330*	9.7/22.6 *15.0*	23.1/29.2 *27.2*	85.2/88.1 *87.0*	1.9/3.6 *2.8*	0.01/0.1 *0.08*	0.01/0.05 *0.03*	-	9.5/11.3 *10.1*
Qtz1-tg2	Aqueous carbonic	-64.6/-39.8 *-55.1*	-23.1 /-17.6 *-22.5*	-5.7/-2.3 *-3.2*	305/344 *320*	21.6/23.8 *23.0*	22.8/25.6 *23.4*	80.7/84.2 *81.0*	2.8/5.2 *3.3*	0.01/0.3 *0.1*	0.01/0.06 *0.04*	-	12.3/16.4 *15.6*
Qtz2-ig	Aqueous carbonic	-45.7/-30.9 *-35.0*	-20.0/-8.4 *-16.0*	-2.5/-1.1 *-2.1*	220/355 *340*	11.9/20.6 *17.0*	25.3/30.0 *27.1*	82.3/89.1 *85.0*	2.4/5.6 *3.0*	0.01/0.3 *0.2*	0.01/0.07 *0.02*	-	10.1/12.8 *11.8*
Qtz2-tg	Aqueous carbonic	-	-3.0/-0.7 *-1.5*	7.3 /12.3 *9.8*	290/330 *300*	0.1/2.4 *1.2*	20.5/27.0 *25.3*	92.3/96.2 *95.0*	2.5/4.1 *3.0*	0.01/0.2 *0.1*	0.05/0.3 *0.1*	0.03/0.07 *0.05*	0.1/2.5 *1.8*
Qtz3-p	Aqueous carbonic	-	-21.7/-9.0 *-17.3*	-2.7/-1.2 *-1.8*	189/308 *265*	12.7/20.9 *18.3*	20.7/23.0 *22.6*	89.2/94.1 *91.0*	1.2/3.2 *2.5*	0.01/0.1 *0.05*	0.01/0.06 *0.04*	- -	5.2/8.8 *6.4*
Qtz-ore-tg	Aqueous	-49.6/-39.6 *-45.0*	-24.3/-14.7 *-21.2*	-	150/248 *210*	18.4/25 *23*	19.6/21.5 *20.5*	83.0/87.0 85.0	-	Trace	-	-	13.0/17.0 *15.0*
Sd-p	Aqueous	-49.0/-40.1 *-44.3*	-23.5/-11.4 *-23.2*	-	110/222 *190*	15.4/24.6 *24.1*	18.8/20.9 *19.4*	80.3/85.6 *83.0*	-	Trace	-	-	15.2/18.3 *17.0*
Brt-p	Aqueous	-59.1/-41.6 *-56.2*	-25.3/-17.7 *-22.4*	-	237/335 *305*	20.7/25.8 *23.0*	21.0/24.0 *23.0*	80.1/84.6 *82.0*	Trace	Trace	Trace	-	12.3/19.2 *18.0*
Cal-p	Aqueous	-	-15.0/-8.0 *-14.0*	-	67/87 *80*	11.8/18.4 *17.0*	18.6/18.9 *18.7*	87.2/89.1 *88.0*	-	-	-	-	10.4/13.1 *12.0*

Table: Microthermometric and compositional data for all generations of fluid inclusions from the Sierra Almagrera (values of mode in italics). - : not determined

Fluid inclusion name	Li	Na	Mg	K	Mn	Fe	Cu	Zn	Sr	Ba	Na/K
Qtz1-tg1	1060	91098	1418	4407	1605	8376	-	523	1028	461	21
	328	69786	-	2936	400	2919	-	193	378	122	24
	543	90418	108	4994	748	5074	-	177	603	217	18
	325	70319	1444	7660	1021	6339	17	479	790	414	9
	202	27260	844	2043	285	7412	20	169	734	222	13
	750	122326	199	3847	730	7102	-	276	1217	215	32
	782	98756	2660	7222	1010	10758	-	360	1240	414	14
	569	73880	2274	3999	489	3161	-	286	641	136	18
Qtz2-tg	0	8198	1719	6347	18	-	-	-	268	13	1
	115	9551	2592	1734	122	-	80	135	104	35	6
Qtz3-p	118	69072	5173	1462	1442	953	31	21	3068	87	47
	126	68540	5236	1326	1563	1028	35	35	2958	80	52
	120	70210	4852	1652	1402	1032	19	15	2500	70	43
	145	67500	4956	1420	1453	856	29	42	2201	68	48
Brt-p	280	47306	1044	7522	310	2093	621	2075	-	-	6
	-	31792	5162	4613	10530	25082	-	4758	-	-	7
	483	63865	1379	6187	329	4438	-	1328	-	-	10
	121	64455	675	9458	842	1660	-	702	-	-	7
	176	45509	1005	4805	-	-	74	1858	-	-	9
	134	34292	511	3698	7	-	32	2124	-	-	9
	169	50607	704	5396	71	-	37	1341	-	-	9
	72	32586	444	7389	-	-	232	2688	-	-	4
	125	21303	121	2629	36	-	94	2577	-	-	8

Table: LA-ICP-MS data for four generations of fluid inclusions from the Sierra Almagrera. Concentrations are given in ppm and Na/K are mass ratios. - : not determined

Vein type	Fluid inclusion petrography	$\delta^{18}O_{host}$ (V-SMOW ‰) min - max *(n)* *median*	$T_{trapping}$ [1] (°C)	$\delta^{18}O_{fluid}$ [2] (V-SMOW ‰) min - max *median*	δD_{fluid} (V-SMOW ‰) min to max *(n)* *median*	$T_{equilibrium}$ [3] min to max (°C)
V-Qtz1	Grain boundary	16.5 - 16.7 *(2)* *16.6*	-	-	–33 to –36 *(2)* *–34.5*	488 - 520
V-Qtz1	Qtz1-tg1+tg2	15.9 - 17.2 *(2)* *16.6*	440 - 480	-	–28 to –30 *(2)* *–29.0*	442 - 478
V-Qtz2	Qtz2-ig	16.2 - 17.0 *(4)* *16.5*	400 - 520	11.7 - 14.2 *12.8*	–23 to –36 *(4)* *–30.0*	404 - 520
V-Qtz2	Qtz2-tg	15.9 - 17.6 *(7)* *16.6*	300 - 560	-	–17 to –48 *(7)* *–34.0*	365 - 704
V-Qtz3	Qtz3-p	14.0 - 14.5 *(2)* *14.3*	250 - 380	5.0 - 9.6 *7.4*	–30 *(1)* *–30*	459
V-ore	Sd-p	20.6 - 22.5 *(4)* *21.5*	120 - 260	3.2 - 14.5 *8.8*	–65 to –80 (*4*) *–71.5*	> 1630
V-ore	Brt-p	13.0 - 13.2 *(2)* *13.1*	280 - 440	8.2 - 11.3 *9.7*	–53 to –69 *(7)* *–58.0*	831 - 1025

[1] Obtained from isochore intersection with PT-path

[2] Equation of Zheng (1993) for quartz-H_2O fractionation; equation of Zheng (1999) for siderite-H_2O and barite-H_2O fractionation

[3] Equation of Suzuoki and Epstein (1976) for muscovite-H_2O fractionation between δD_{fluid} and $\delta D_{host\text{-}rock}$ = –52‰

Table: Isotopic data for various stages of fluid inclusions from the Sierra Almagrera, - : not determined.